

NASA/TM-2015-218697



Internal Structural Design of the Common Research Model Wing Box for Aeroelastic Tailoring

Christine V. Jutte
Craig Technologies Inc., Hampton, Virginia

Bret K. Stanford and Carol D. Wieseman
Langley Research Center, Hampton, Virginia

March 2015

NASA STI Program . . . in Profile

Since its founding, NASA has been dedicated to the advancement of aeronautics and space science. The NASA scientific and technical information (STI) program plays a key part in helping NASA maintain this important role.

The NASA STI program operates under the auspices of the Agency Chief Information Officer. It collects, organizes, provides for archiving, and disseminates NASA's STI. The NASA STI program provides access to the NTRS Registered and its public interface, the NASA Technical Reports Server, thus providing one of the largest collections of aeronautical and space science STI in the world. Results are published in both non-NASA channels and by NASA in the NASA STI Report Series, which includes the following report types:

- **TECHNICAL PUBLICATION.** Reports of completed research or a major significant phase of research that present the results of NASA Programs and include extensive data or theoretical analysis. Includes compilations of significant scientific and technical data and information deemed to be of continuing reference value. NASA counter-part of peer-reviewed formal professional papers but has less stringent limitations on manuscript length and extent of graphic presentations.
- **TECHNICAL MEMORANDUM.** Scientific and technical findings that are preliminary or of specialized interest, e.g., quick release reports, working papers, and bibliographies that contain minimal annotation. Does not contain extensive analysis.
- **CONTRACTOR REPORT.** Scientific and technical findings by NASA-sponsored contractors and grantees.

- **CONFERENCE PUBLICATION.** Collected papers from scientific and technical conferences, symposia, seminars, or other meetings sponsored or co-sponsored by NASA.
- **SPECIAL PUBLICATION.** Scientific, technical, or historical information from NASA programs, projects, and missions, often concerned with subjects having substantial public interest.
- **TECHNICAL TRANSLATION.** English-language translations of foreign scientific and technical material pertinent to NASA's mission.

Specialized services also include organizing and publishing research results, distributing specialized research announcements and feeds, providing information desk and personal search support, and enabling data exchange services.

For more information about the NASA STI program, see the following:

- Access the NASA STI program home page at <http://www.sti.nasa.gov>
- E-mail your question to help@sti.nasa.gov
- Phone the NASA STI Information Desk at 757-864-9658
- Write to:
NASA STI Information Desk
Mail Stop 148
NASA Langley Research Center
Hampton, VA 23681-2199

NASA/TM-2015-218697



Internal Structural Design of the Common Research Model Wing Box for Aeroelastic Tailoring

Christine V. Jutte
Craig Technologies Inc., Hampton, Virginia

Bret K. Stanford and Carol D. Wieseman
Langley Research Center, Hampton, Virginia

National Aeronautics and
Space Administration

Langley Research Center
Hampton, Virginia 23681-2199

March 2015

The use of trademarks or names of manufacturers in this report is for accurate reporting and does not constitute an official endorsement, either expressed or implied, of such products or manufacturers by the National Aeronautics and Space Administration.

Available from:

NASA STI Program / Mail Stop 148
NASA Langley Research Center
Hampton, VA 23681-2199
Fax: 757-864-6500

Abstract

This work explores the use of alternative internal structural designs within a full-scale wing box structure for aeroelastic tailoring, with a focus on curvilinear spars, ribs, and stringers. The baseline wing model is a fully-populated, cantilevered wing box structure of the Common Research Model (CRM). Metrics of interest include the wing weight, the onset of dynamic flutter, and the static aeroelastic stresses. Twelve parametric studies alter the number of internal structural members along with their location, orientation, and curvature. Additional evaluation metrics are considered to identify design trends that lead to lighter-weight, aeroelastically stable wing designs. The best designs of the individual studies are compared and discussed, with a focus on weight reduction and flutter resistance. The largest weight reductions were obtained by removing the inner spar, and performance was maintained by shifting stringers forward and/or using curvilinear ribs: 5.6% weight reduction, a 13.9% improvement in flutter speed, but a 3.0% increase in stress levels. Flutter resistance was also maintained using straight-rotated ribs although the design had a 4.2% lower flutter speed than the curved ribs of similar weight and stress levels were higher. For some configurations, the differences between curved and straight ribs were smaller, which provides motivation for future optimization-based studies to fully exploit the trade-offs.

Nomenclature

ε	Distance between two structural members
η	Fraction that determines control line endpoint locations in a wing section
CG	Center of gravity
CG _{root}	Center of gravity at the root region (first 1/8 of wing semi-span)
CG _{tip}	Center of gravity at the tip region (last 1/8 of wing semi-span)
CRM	Common Research Model
FGM	Functionally graded materials/metals
i or IBD	Inboard wing section
KS	Kreisselmeier-Steinhauser function
LE	Leading edge
o or OBD	Outboard wing section
$p1_i, p1_o$	Number of structural members within a wing section
$p1^*$	Vector defining spanwise structural members as spars or stringers
$(p2_i, p3_i), (p2_o, p3_o)$	Control line parameters in a wing section
$[p4_i, p5_i, p6_i], [p4_o, p5_o, p6_o]$	Curvature definition parameters in a wing section
$p7_i, p7_o$	Rib rotation parameter
TE	Trailing edge
x	Direction parallel to the aircraft fuselage centerline
y	Direction parallel to ground and perpendicular to the aircraft fuselage centerline

I. Introduction

Curvilinear spars, ribs, and stiffeners may offer advantages over the conventional straight spar and rib designs utilized in most aircraft today in that they widen the structural design space. The traditional orthogonal grid of structural members typically has disparate load-bearing requirements during flight, whereas curvilinearity will blend these roles, potentially enhancing efficiency. Additionally curvilinear members may prove to be advantageous in coupling wing bending and torsional stiffness for improved aeroelastic tailoring as well. New additive

manufacturing techniques, such as the electron beam freeform fabrication (EBF³) [1] are also maturing, providing more opportunities for fabricating these potentially complex lightweight structures.

Curvilinear structural reinforcement of wing structures has been readily demonstrated at the panel level, with the majority of the work conducted by Kapania and coworkers at Virginia Tech. Curved metallic panel stiffeners have been shown to improve the performance of a minimum-mass panel under buckling, crippling, and strength constraints [2], [3]. Locatelli et al. [4] expands the concept to the wing box level, using full-depth curvilinear ribs and spars. Curvilinear structures are again shown to effectively minimize wing weight under a variety of constraints, though aeroelastic physics and metrics are not considered. Finally, though Refs. [5], [6], and [7] do not utilize a curvilinear parameterization, all demonstrate a benefit in structural weight/performance due to a deviation from the traditional orthogonal grid of metallic ribs and spars within a wing box.

NASA is working with Kapania and coworkers at Virginia Tech to support the development of an optimization tool that populates a transport aircraft wing with curvilinear spars, ribs, and stiffeners for improved structural efficiency and aeroelastic performance. The curvilinear stiffeners will replace traditional stringers to more directly reinforce individual skin panels. In parallel to the development of this optimization tool, the work presented in this paper explores the design space in a more methodical manner to better understand a transport wing's aeroelastic response when various perturbations are made to its design.

In this report, a fully-populated wing box structure within the Common Research Model (CRM) wing [8] is used as a baseline. An aeroelastic framework of MATLAB, PATRAN, and NASTRAN modules is used to compute the static aeroelastic response and the dynamic aeroelastic flutter boundary of a given wing structure. These concepts are described in Section II. Section III describes the parameterization of the internal structural members of the wing box. Twelve parametric studies are performed on the baseline's spars, ribs, and stringers to observe which design changes in the internal structure have the greatest effect on both increasing the wing's flutter resistance and in decreasing its weight. The first five studies, described in Section III, modify the stringers and inner spar, while keeping the baseline rib configuration constant. The next six studies, described in Section V, modify the ribs, while keeping the baseline spar/stringer configuration constant. Section VI presents the final study which combines spar designs with rib designs of the previous studies. In section VII, additional evaluation metrics are considered to identify design trends that lead to lighter-weight, aeroelastically stable wing designs, where the results are specific to the CRM and similar wing designs. Section VIII compares the best designs of the individual studies (1-12) and illustrates which spar and rib configurations are most effective. Section IX of this paper provides the final conclusions and outlook.

II. Modeling and Baseline Description

The transport aircraft wing configuration used for this work is the Common Research Model, which is a full-scale, cantilevered wing. The CRM is a modern single-aisle transport class aircraft configuration that was generated as an open geometry for collaborative research within the aerodynamics community. It has a wingspan of 192.8 ft, an aspect ratio of nine, a taper ratio of 0.275, a leading edge sweep angle of 35°, and a break along the trailing edge at 37% of the semi-span (also referred to as a yehudi break) [8]. A traditional internal structure was developed in this work to use as a baseline for structural analysis. The wing box was defined to lie between 10% and 70% of the local chord.

The baseline wing box topology used for this work is shown in Figure 1 and consists of full-depth spars at the box leading edge, trailing edge, and one-third of the distance between the two. Thirty-seven straight ribs are evenly distributed from root to tip, each aligned with the airflow. Seven pairs of stringers (one on each skin) travel from root to tip: two pairs are evenly distributed between the leading edge spar and the inner spar, and five pairs between the inner and trailing edge spar. These stringers have a rectangular cross section, with a depth of 2.95 inches and a thickness of 0.18 inches. A full-depth rib stiffener exists at each stringer-rib intersection, each with a depth of 2.64 inches and a thickness of 0.18 inches.

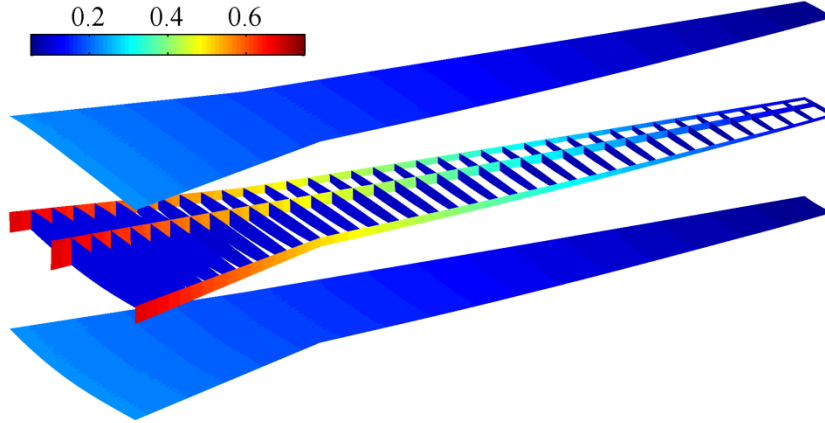


Figure 1. Baseline CRM structure used for tailoring studies: contour indicates local shell thickness (inches).

The thickness distribution of the ribs, spars, and wing skins is seen in the figure, and aluminum (2024-T3 alloy) was used throughout. Spars, ribs, and skins were modeled with higher-ordered triangular shell elements, stringers and rib stiffeners were modeled with beam elements, and the displacement degrees of freedom of all nodes at the wing-root of Figure 1 were fixed to zero. The inertial impact of leading and trailing edge control effectors were modeled as lumped masses, connected to the leading and trailing edge spars via un-weighted interpolation elements. Six 320 lb masses were used along the inboard leading edge, and three additional of 240 lbs outboard. Similarly, six 840 lb masses and three 140 lb masses were used along the trailing edge. These mass values were calculated by scaling data from a similar commercial transport.

Starting with the outer mold line of the CRM [8], MATLAB scripts were used to generate PATRAN session files to populate the CRM outer mold line with a user-defined topology of ribs, spars, stringers, and rib-stiffeners (all of which may be curvilinear or straight). The resulting geometry was auto-meshed using CTRIAR elements (ribs, spars, and skins) and CBAR elements (stringers and rib stiffeners) to define the finite element model. A static aeroelastic analysis, buckling analysis, and a flutter analysis were then conducted in NASTRAN. MATLAB scripts were used to generate input files for the analyses and to extract the data from the NASTRAN output files to compare performance metrics and assess the aeroelastic tailoring concepts. Flat-plate aerodynamic paneling was utilized for both steady and unsteady air loads, with a 10×10 mesh of boxes for the inboard section of the wing (spanning from the root to the yehudi break) and a 10×40 mesh for the outboard wing section (spanning from the yehudi break to the tip). Finite element nodes located at intersections of the upper skins and ribs, or the upper skins and spars, were used to interpolate between the structural and aerodynamic meshes.

Static aeroelastic wing deformation was computed at specified angles of attack of -2° , 0° , 2° , 4° , and 6° , a Mach number of 0.85, and an altitude of 35 kft. The resulting data set was distilled into structural weight, wing tip deflection/twist and an aggregate stress metric (Kreisselmeier-Steinhauser (KS) function [9]), where low values are desirable. The flexural axis of the wing [10] and the line of centers of gravity from root to tip were also computed. Buckling eigenvalues were computed for each deformed state and the corresponding buckling mode. This can be done for each of the aeroelastic trim cases, but only the extremes (-2° and 6°) are typically of interest. A flutter analysis (p-k method) was then performed with 20 structural dynamic modes at a Mach number of 0.85, and using the speed of sound at sea level, the velocity was computed and fixed. The dynamic pressure varied from 0 to 14.8 psi and was divided into 250 increments by varying the flow density; zero-damping cross-over points indicate flutter.

The resulting weights and flutter dynamic pressures for the design permutations provided in this report are normalized by the baseline wing model's metrics. A higher value of the normalized flutter dynamic is desired, providing a greater margin between the cruise dynamic pressure and the flutter boundary.

III. Solution Methodology

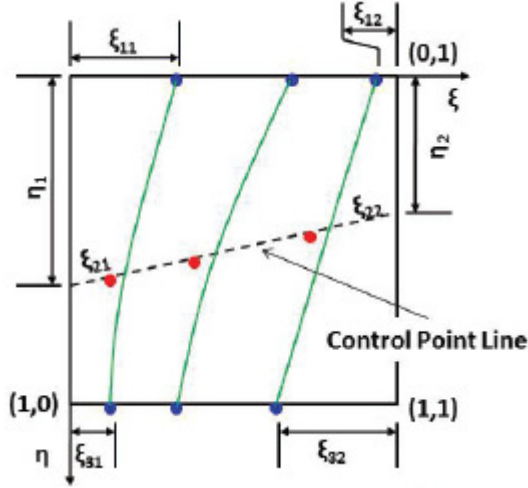
In this work, twelve parametric studies are performed on the baseline CRM wing's internal structure, leaving the material and overall thicknesses the same as the baseline, but altering the number, location, orientation, and curvilinearity of the ribs and spars. A brief description of the studies is included in Table 1; the last column refers to designs highlighted later in Figure 33.

Table 1. Description of the parametric studies performed on the spars and ribs.

Study	Investigations	Designs in Figure 33
	Spar studies	
1	Number of straight spars and their location	
2	Curvature of inner spar (higher degree of curvature than study 3)	a, b
3	Curvature of inner spar (lower degree of curvature than study 2)	c
4	Curvature of stringers only (inner spar removed)	d, e
5	Varying stringer curvature separately in inboard and outboard (inner spar removed)	
	Rib studies	
6	Number of straight ribs	
7	Rotating straight ribs (inboard and outboard orientations the same)	g
8	Rotating straight ribs (only outboard orientation modified)	
9	Rib curvature (same curvature for inboard and outboard)	h, i
10	Study 9 but with inner spar removed	j, k, l
11	Rib curvature (different curvature for inboard and outboard)	
	Combined studies	
12	Combines spar/stringer designs (studies 1-5) with rib designs (studies 6-11)	m, n

In these studies, the geometry of a few specific structural members was fixed, including the front and rear spars, one rib at the wing yehudi break, one rib at the wing tip, and the skins. The baseline wing box was defined using a series of parameters in order to facilitate the generation of alternate wing designs. For each new design, a MATLAB script generated a set of session files for PATRAN to create a new CAD model of the internal wing box configuration and its corresponding finite element mesh. It was not uncommon for PATRAN to have complications meshing a design or creating the CAD surfaces. Meshing issues often occurred when the alignment of two structural members within a design caused highly skewed elements. Therefore, it was advantageous to study as many designs as possible to help minimize the effect of missing data points (gaps in the design space). To thoroughly explore the design space without committing to the numerous function evaluations required of a formal optimization routine, a full factorial approach [11] was used when applicable.

The internal rib and spar structure of the baseline CRM was parameterized using the ‘linked shape parameterization’ as described in [12], which defines the structural members (either ribs or spars) of a wing section using b-splines. The schematic in Figure 2 shows three b-splines in the unit square, where each spline has three control points: one on the upper edge of the design space, one on the dashed line called the control line (which determines the location of maximum curvature for each structural member), and one on the lower edge of the design space. The placement of all of the control points within the design space is defined by six parameters, p1-p6, where p1 simply defines the number of b-splines (or structural members). Parameters p2-p3 (referred to in this work as the *control line parameters*) define the locations of the endpoints of the control line. These two parameters, along with an equation in [12] and parameter p5, determine the location of the inner of three control points defining a structural member; this inner point falls on the control line. Parameters p4 and p6 define the locations of the remaining two control points located at the endpoints of each structural member. Together, parameters p4, p5, and p6 are referred to in this work as the *curvature definition parameters*. This unit square of Figure 2 is mapped to a section of the wing whose perimeter is defined as a quadrilateral.



Parameter	Description
p_1	Number of <i>SpaRibs</i>
p_2	η_1
p_3	η_2
p_4	ξ_{12} / ξ_{11}
p_5	ξ_{22} / ξ_{21}
p_6	ξ_{32} / ξ_{31}

Figure 2. ‘Linked shape parameterization’ (Courtesy of authors of Ref. [12]).

The CRM baseline model has two wing sections, the inboard (IBD) and outboard (OBD). The ‘linked shape parameterization’ is applied twice to the inboard, once for spars and once for ribs, and twice to the outboard, once for the spars and once for the ribs, leading to a total of 24 design variables. Figure 3 shows how the ‘linked shape parameterization’ is mapped to the CRM baseline model for both the spars (Figure 3(a)) and ribs (Figure 3(b)). Inboard parameters are labeled with an “i” subscript, while parameters in relation to the outboard are labeled with an “o” subscript. Referencing the figure, each structural member is defined by three control points, as mentioned above. Since the spars run spanwise from root to tip, each spar is comprised of two consecutive b-splines, one from each wing section. For continuity, the inboard parameter at the wing break (p_{6_i}) and the outboard parameter at the wing break (p_{4_o}) are coincident; and therefore, p_{4_o} is not an independent parameter in the CRM parameterization. When referring to the general shape of a spar, five curvature definition parameters which span both wing sections are used, i.e. [p_{4_i} , p_{5_i} , p_{6_i} , p_{5_o} , p_{6_o}]. The locations of the control points associated with p_{5_i} and p_{5_o} will slightly change as the endpoints of the control lines are varied by parameters [p_{2_i} , p_{3_i}] and [p_{2_o} , p_{3_o}], respectively. For the ribs, the general shape is defined by three curvature definition parameters, i.e. [p_4 , p_5 , p_6], where the location of the control points associated with p_5 will slightly change as parameters p_2 and p_3 are updated, within the respective wing section.

Figure 4 provides an example of how the six parameters (p_1 - p_6) define ribs within a wing section. In the example, the number of ribs equals three, and the first control point of each structural member is located on the leading edge. The second control point is located on the control line, and the third control point is located on the trailing edge. The curvature definition parameters (p_4 - p_6) can define whether the structural members in the wing section are convex or concave. For the CRM application, the convex ribs open toward the wing tip (when p_4 and p_6 are greater than p_5), while concave ribs open toward the wing root, (when p_4 and p_6 are less than p_5). Therefore, in this rib example, the curves are convex. The control line parameters define the endpoints of the control line and, in this example, provide a unique shape for each rib due to the varying locations of each rib’s maximum curvature.

When the values of the curvature definition parameters (p_4 - p_6) are equal, the structural members are straight. Figure 5 illustrates six designs (1a-2c) having straight members. When the p_4 - p_6 values for a structural member all equal unity, for example [p_{4_i} , p_{5_i} , p_{6_i} , p_{5_o} , p_{6_o}] = [1, 1, 1, 1, 1] for spars and [p_4 , p_5 , p_6] = [1, 1, 1] for ribs, the straight members are all equally spaced (illustrated as (1a) and (2a), respectively). For the spars, when all the values are greater than unity, for example [4, 4, 4, 4, 4], the straight spars are unequally spaced and shifted toward the leading edge, as shown in (1b). The exact spacing between the members is determined by an equation found in [12]. When all the values are less than unity, for example [0.25, 0.25, 0.25, 0.25, 0.25], the straight spars are unequally spaced and shifted toward the trailing edge, as shown in (1c). For the ribs, when all the values are greater than unity, for example [4, 4, 4], the straight ribs are all unequally spaced and shifted toward the wing tip, as shown in (2b). When all the values are less than unity, for example [0.25, 0.25, 0.25], the straight ribs are all unequally spaced and shifted toward the wing root, as shown in (2c).

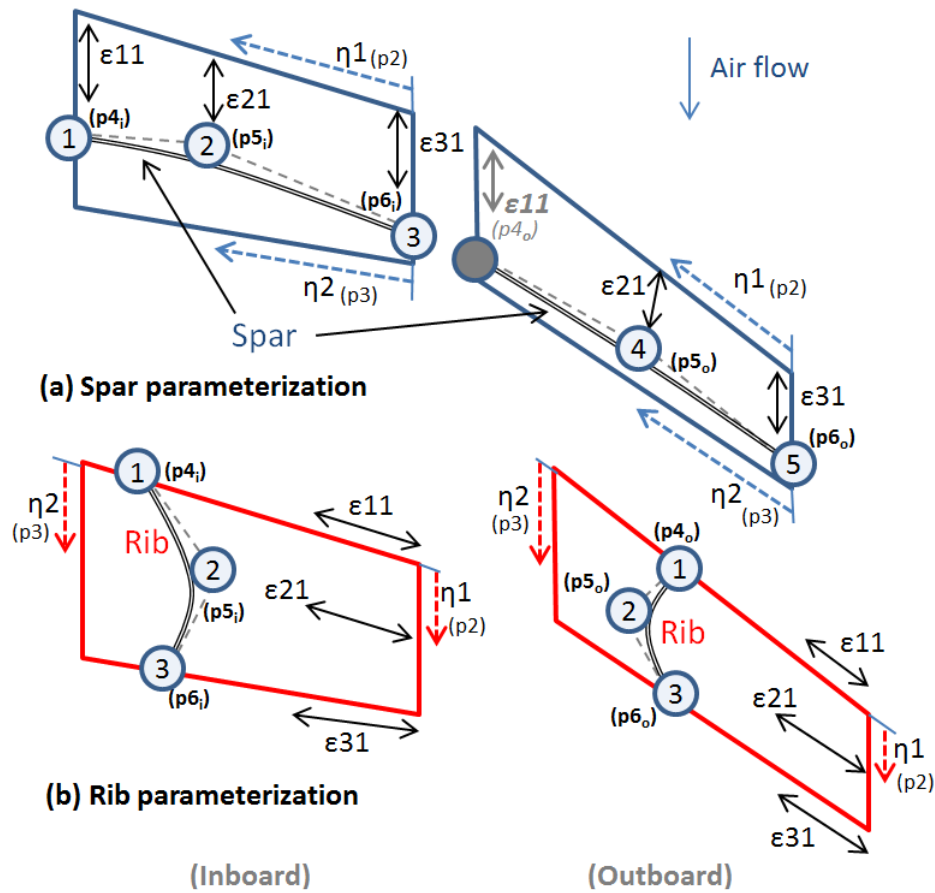


Figure 3. Application of the ‘linked shape parameterization’ (p1-p6) in both sections of the CRM wing box. The parameters define 5 control points (noted as circles) for each spar and 3 control points (noted as circles) for each rib. The arrows for the epsilon values are representative of their location in the parameterization but not their actual length in this example. For clarity, the control lines are not explicitly shown.

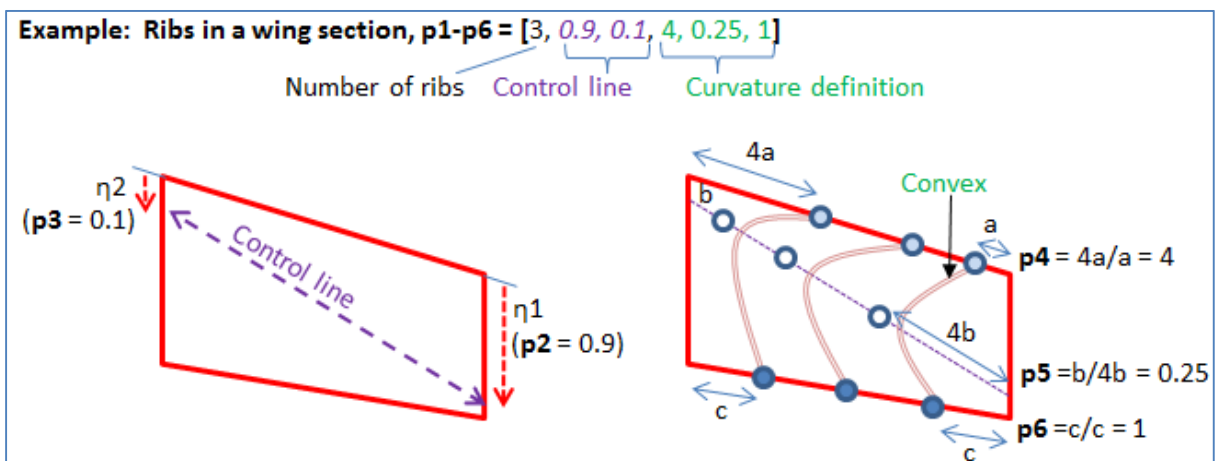


Figure 4. An example of the application of ‘linked shape parameterization’ for defining ribs within a wing section.

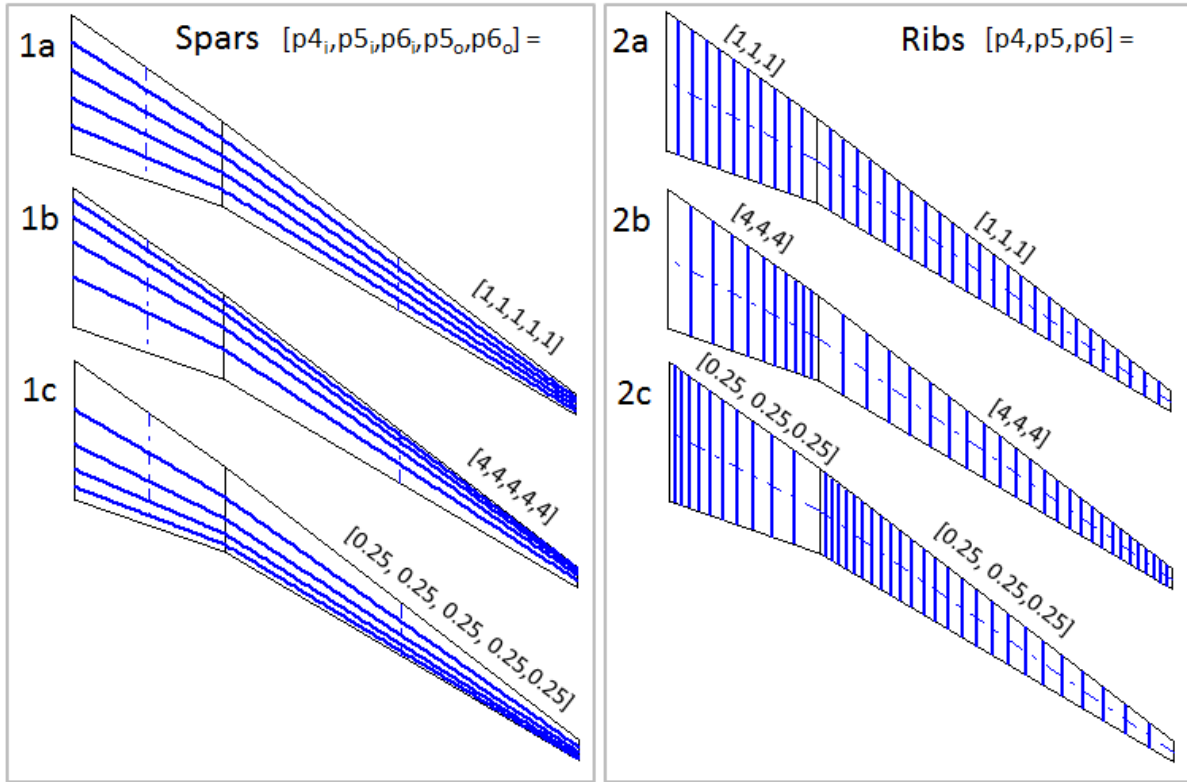


Figure 5. Illustration of how the values of the curvature definition parameter (p4-p6) can create straight structural members with various spacings.

When the values of the curvature definition parameters (p4-p6) are unequal to one another, the structural members are no longer straight. Figure 6 shows the effect of parameters p4-p6 on four spars when the parameters are not equal. The control lines, shown as the dashed lines, are the same as the baseline's, (p2=p3=0.5). The outboard wing section of the left figure happens to have straight spars since p6_i=p5_o=p6_o. Similarly, Figure 7 shows the effect of parameters p4-p6 on rib shape, recalling that the parameter values can define convex or concave ribs. In the figure, the control lines for the ribs are located along the mid-chord, in the same location as the baseline's control lines, (p2=p3=0.5).

In these studies, the control line is varied using five pairs of values for the control line parameters, p2 and p3. The five pairs of values are shown at the bottom of Table 2 and are represented within the table by dashed lines. The top row illustrates the effect that each pair of control line parameters has on a set of four spars within the inboard wing section, where the curvature definition parameters are constant over the entire row at [p4_i, p5_i, p6_i] = [4, 0.25, 4]. The same is shown for the ribs but using a different set of curvature definition parameters, [p4_i, p5_i, p6_i] = [1, 4, 1].

The baseline CRM wing was introduced in section II. Its corresponding parameters are shown in Table 3, along with a schematic of the wing box in Figure 8. Since the baseline's ribs are straight and uniformly spaced and the inner spar is straight (at least within each wing section), the curvature definition parameters (p4-p6) are all equal to unity. The baseline's control lines in each wing section are defined with p2=p3=0.5, which means the spar control lines are located along the mid-span of each wing section, while the rib control lines are located along the mid-chord of each section.

A few additional parameters were added to the 'linked shape parameterization' to facilitate further design investigations. First, the stringers of the baseline CRM model were incorporated into the parametric model by replacing a single spar with a pair of stringers (one on the upper skin and one on the lower skin). The spars and stringers are associated in that the stringers take on the same location and shape as the spar it replaces. Therefore, by introducing an additional parameter, p1*, which is a binary vector whose length is the total number of spars and stringers, the members can be toggled between a full depth design (spars) and a partial depth design (stringers), where spars = 1 and stringers = 0. For the baseline model, the third member (of eight members total) was defined as

a spar while all the other members were stringers, i.e. $p1^* = [00100000]$. An additional parameter, $p7$, was also added to the ribs to populate the section with straight ribs at a specified angle of orientation, since the 'linked shape parameterization' had limitations in this regard. When using this parameter (which was not used for the baseline), the rib definition parameters ($p2$ - $p6$) are ignored since the rotated ribs have no curvature.

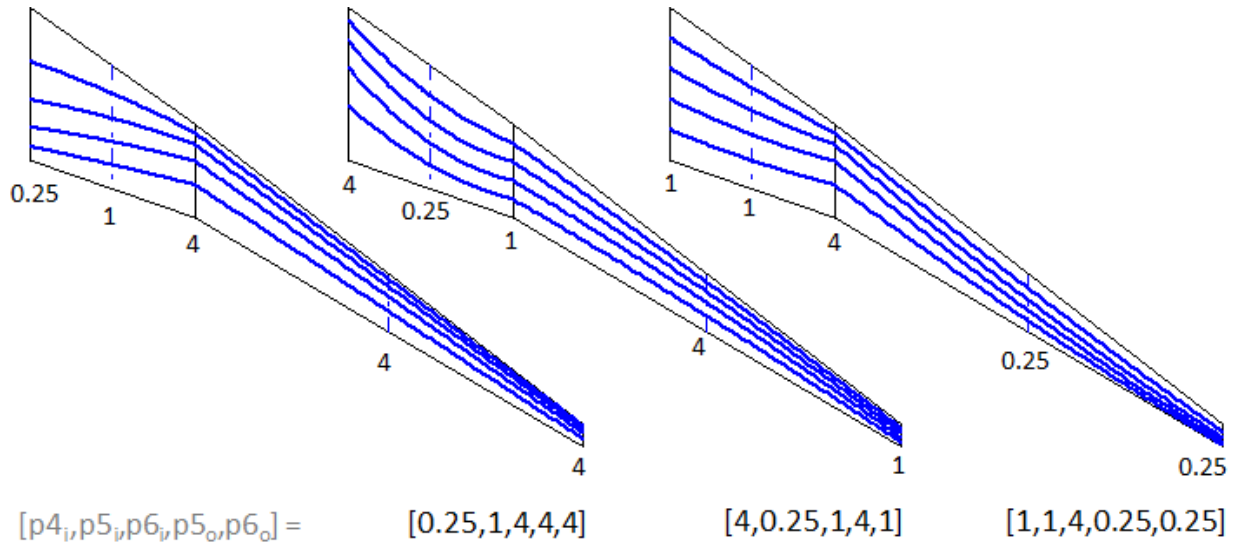


Figure 6. Three examples showing the effect of parameters $p4$ - $p6$ (more specifically $[p4_i, p5_i, p6_i, p5_o, p6_o]$) on the spar designs.

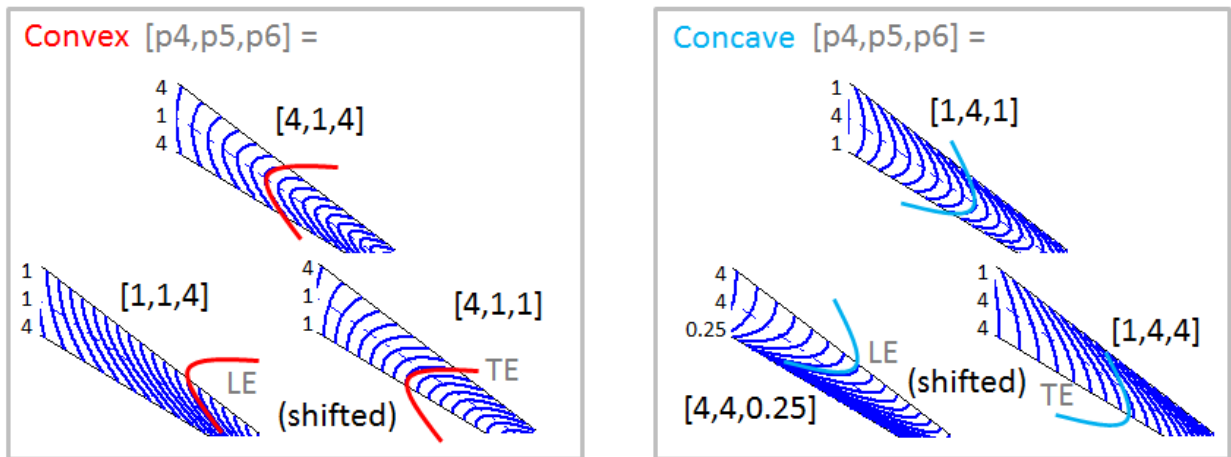
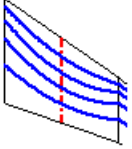
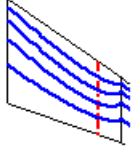
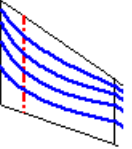
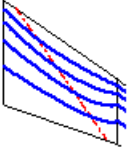
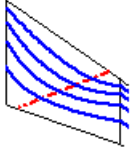
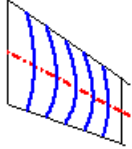
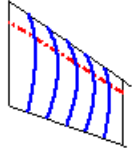
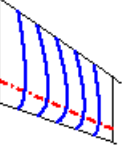
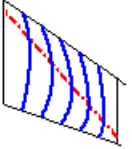
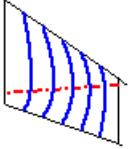


Figure 7. Six examples showing the effect of parameters $p4$ - $p6$ on the rib designs. Certain combinations of values can shift the curves toward the leading edge (LE) or trailing edge (TE).

Table 2. Examples showing the effect of the control line (dashed) on a constant set of curvature definition parameters (p4-p6) for spars and ribs in the inboard.

Spars					
Example [p4 _i , p5 _i , p6 _i] = [4, 0.25, 4]					
Ribs					
Example [p4 _i , p5 _i , p6 _i] = [1, 4, 1]					
[p2, p3]	[0.5, 0.5]	[0.2, 0.2]	[0.8, 0.8]	[0.9, 0.1]	[0.1, 0.9]

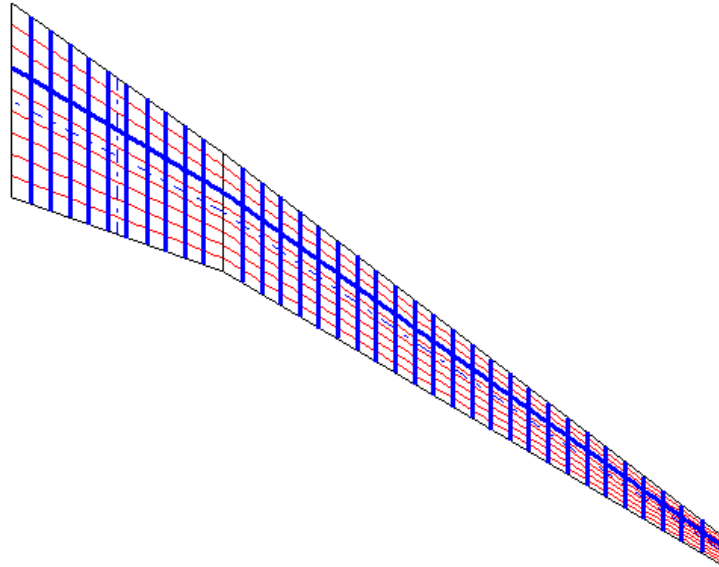


Figure 8. Schematic of the baseline CRM model, where the thick lines represent the parameterized spars and ribs, the dashed lines represent the control lines, and the solid thin red lines represent the stringers. Stringers were incorporated into the baseline model using an additional parameter, p1*.

Table 3. Parameters for the baseline CRM model.

	Parameters	Baseline Values
Spars/stringers	p1*	[00100000]
IBD Spars/stringers	[p1, p2, p3, p4, p5, p6]	[8, 0.5, 0.5, 1, 1, 1]
OBD Spars/stringers	[p1, p2, p3, p5, p6]	[8, 0.5, 0.5, 1, 1]
IBD Ribs	[p1, p2, p3, p4, p5, p6], p7	[10, 0.5, 0.5, 1, 1, 1], N/A
OBD Ribs	[p1, p2, p3, p4, p5, p6], p7	[25, 0.5, 0.5, 1, 1, 1], N/A

IV. Spar and Stringer Topology Studies

In this section, five parametric studies are performed on the spars and stringers. Using the parameterization described above, the spars and stringers are associated with one another. Therefore, it is not possible to only vary the inner spar's shape without also varying the stringers' shape. However, it is possible to exclude the inner spars and study the effect of only using stringers. The first three parametric studies focus on spars and stringers (referred

to as spar/stringer studies), while the last two consider stringers only. An alternative stringer configuration, run-out stringers, does not have a geometric dependence on the spars and often times cross over and intersect with the spars. Run-out stringers were briefly implemented in this work, but the intersections created highly skewed elements often causing meshing errors (and therefore are not used here).

A. Number and Location of Straight Spars

The first parametric study explores how the number of straight spars and their location affect wing weight and the flutter speed. As mentioned before, the baseline design has eight equally spaced spanwise structural members where all the members are stringers except for the third member, which is a spar. In this study, the total number of spanwise structural members is always eight, like the baseline. Only the binary values in parameter $p1^*$, which identifies each spanwise structural member as a spar or a pair of stringers, is modified as delineated in Table 4, (where this table is included for consistency purposes as each subsequent study will have a similar table). Figure 9 shows the normalized weight and normalized flutter dynamic pressure results with respect to the baseline; designs are distinguished from one another as described in the key. With a change in spar location, both the mass and stiffness (and their distributions within the wing) are modified. For the most part, the results show that the addition of spars increases the flutter speed. In every case, as the number of spars is held constant, the flutter speed increases when the spars are moved forward, while the opposite occurs when the spars move aft. The effect is significant enough that the design with four spars all positioned toward the leading edge has the same flutter speed as the design with eight spars. This type of tailoring technique, i.e., moving the center of gravity (CG) forward especially at the outboard, is well-known for flutter speed improvement [13].

Table 4. Study 1: number and location of spars.

	Modified parameters	Parameter values
Distinction between a spar and a stringer	$p1^*$	0's or 1's

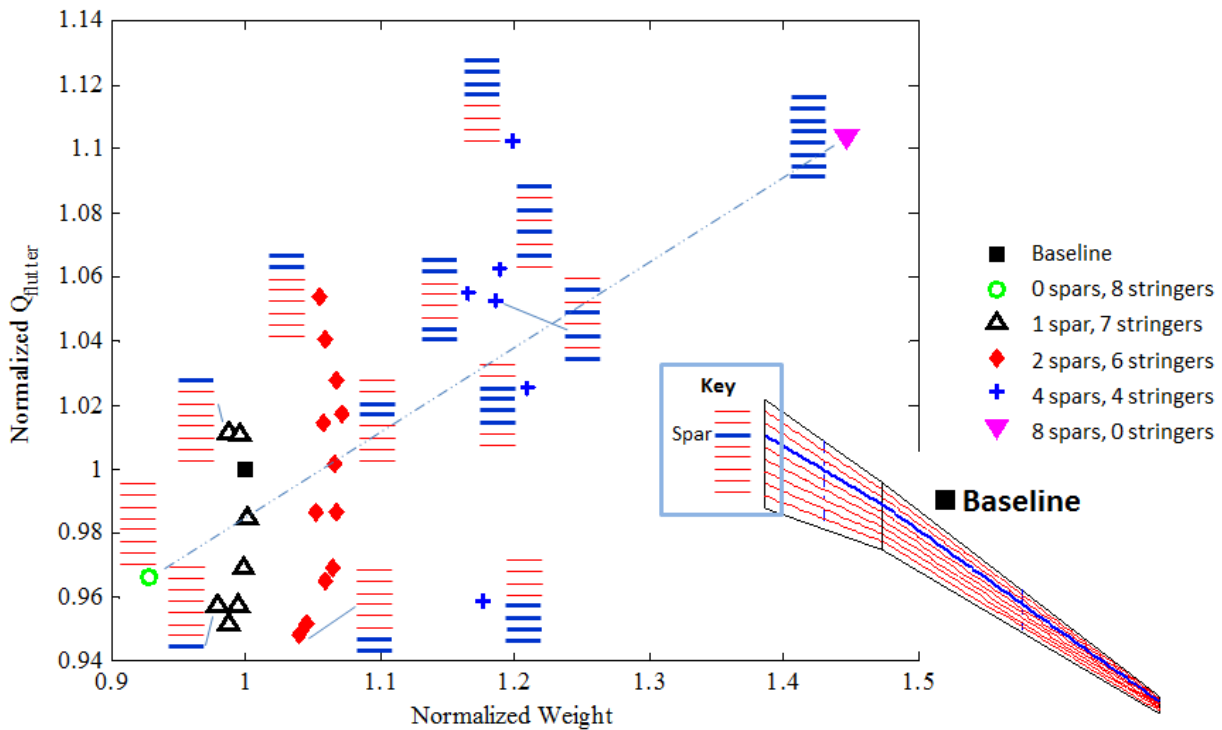


Figure 9. Results of the studies on the number of spars and their location (study #1). Data is normalized by the baseline model's weight and flutter dynamic pressure.

B. Spar Curvature

The next two parametric studies (#2 and #3) explore how the curvature definition of spar/stringers (represented by $[p4_i, p5_i, p6_i, p5_o, p6_o]$) affect wing weight and flutter speed. The values used for each parameter are shown in Table 5 and Table 6. The only difference between these studies is that the values in study #2 more dramatically shift the spar/stringer control points either closer to the leading edge (when using 10 instead of 4) or closer to the trailing edge (when using 0.1 instead of 0.25). A full factorial study would have considered 243 (3^5) permutations; however, given the results in the previous study, which showed better stability when the spars were closer to the leading edge, designs having all the spar's control points shifted toward the trailing edge, i.e., $[p4_i, p5_i, p6_i, p5_o, p6_o]$ all ≤ 1 (except the baseline), were not considered in this study.

Figure 10 shows the results compared to the baseline design for these two studies. Interestingly, there is minimal trade-off between weight and flutter speed. After analyzing the scatter of permutations, a trend between the curvature definition parameters and the flutter speed was identified by sorting the scatter by the last two parameters, $p5_o$ and $p6_o$, as indicated by the figure's legends. In other words, the flutter speed was influenced most by the position of the two control points located closest to the wing tip, where positioning toward the leading edge resulted in higher flutter speed, and vice versa. Once again, the shift of the CG forward greatly affects the flutter speed, especially at the wing tip [13]. Among the resulting designs, study #2 included a design where the spar was straight and also shifted toward the leading edge, i.e. the curvature definition parameters were $[10, 10, 10, 10, 10]$. This design (noted as 'a' in Figure 10) performs just as well as the other designs which all have curvature in the spars. However, in shifting the spars and stringers toward the leading edge, the trailing edge is not well supported by the stringers (which is analogous to '1b' in Figure 5). By using spars and stringers equally spaced in the inboard, $[p4_i, p5_i, p6_i] = [1, 1, 1]$, but still curve toward the leading edge as they approach the wing tip for the purpose of flutter resistance, $[p5_o, p6_o] = [10, 10]$, other considerations such as skin buckling may be improved using curvilinear spar/stringers. For example, the design with no curvature, i.e. $[10, 10, 10, 10, 10]$, has a higher flutter speed than the baseline but a 10% drop in buckling resistance, where a design with curvature, i.e. $[1, 1, 1, 10, 10]$ (depicted as design 'b' in the figure), has the same buckling resistance as the baseline and still has a higher flutter speed than the baseline. Finally, between the two studies, study #2 has greater biasing due to its parameter values and also achieves a larger range of flutter speeds.

Table 5. Study 2: spar and stringer curvature (more curvature potential).

	Modified parameters	Parameter values
Curvature definition	$p4_i, p5_i, p6_i, p5_o, p6_o$	0.1, 1, or 10

Table 6. Study 3: spar and stringer curvature (less curvature potential).

	Modified parameters	Parameter values
Curvature definition	$p4_i, p5_i, p6_i, p5_o, p6_o$	0.25, 1, or 4

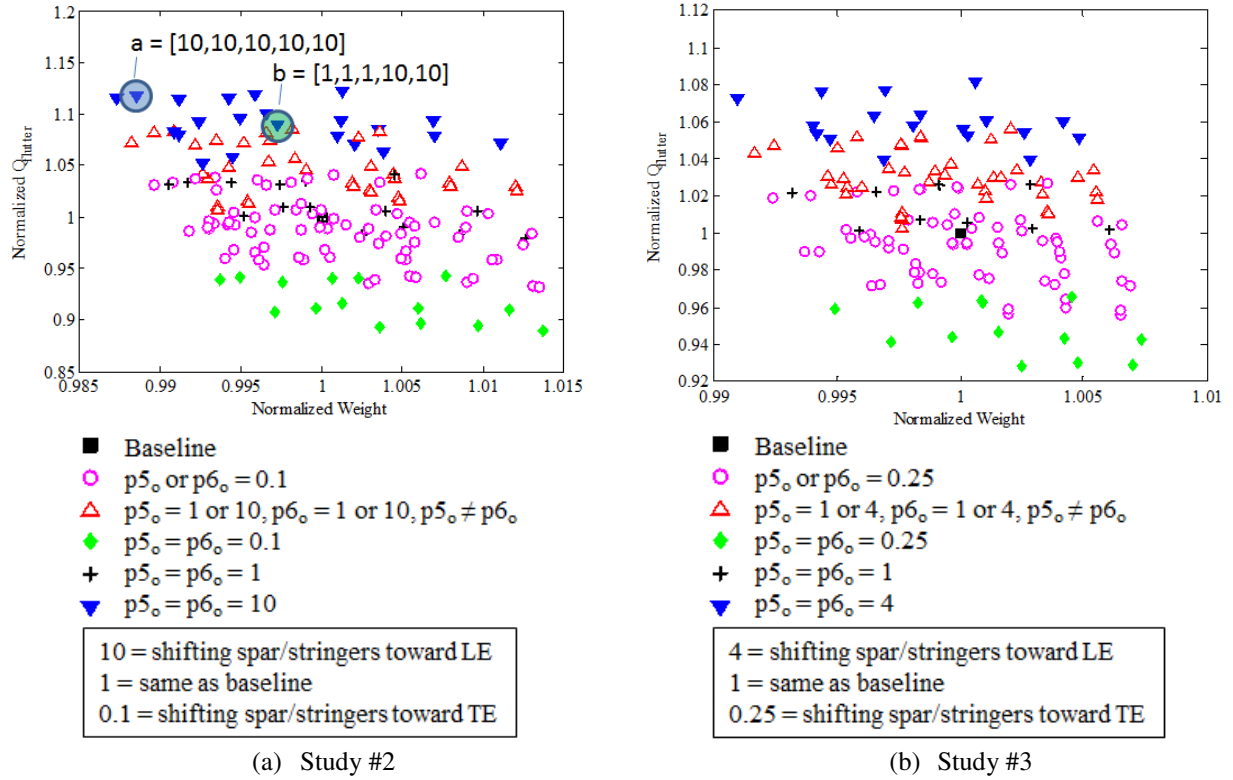


Figure 10. Results of the spar curvature studies (study #2 and #3).

C. Stringer Curvature

The next two parametric studies remove the inner spar to investigate the effects of stringers only. Instead of comparing to the baseline design, the designs in this study are compared to a design identical to the baseline but with no inner spar and a total of 8 pairs of stringers. The first of the two studies (study #4) explores how stringer curvature affects wing weight and the flutter speed. The values used for each parameter are described in Table 7 and were identical to those used in study #3. Figure 11 shows the results compared to a design with 8 straight stringers. Similar to the spar studies above, the flutter speed is influenced most by the position of the two control points located closest to the wing tip ($p5_o$ and $p6_o$), where positioning toward the leading edge results in higher flutter speed. As compared to study #3, which includes an inner spar and uses the same curvature definition values (0.25, 1, and 4), the range in flutter speeds and weight is slightly less when the spar is not present.

Table 7. Study 4: stringer curvature, $p1^* = [00000000]$.

	Modified parameters	Parameter values
Curvature definition	$p4_i, p5_i, p6_i, p5_o, p6_o$	0.25, 1, or 4

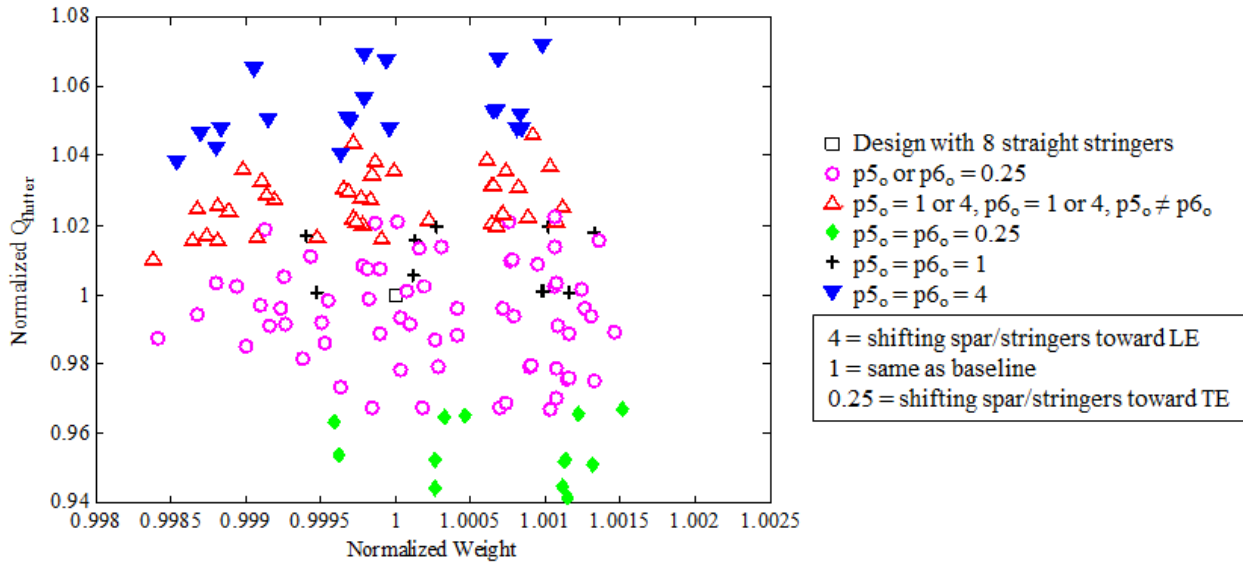


Figure 11. Results of the stringer curvature study (study #4).

The next parametric study (#5) investigates the effects of varying the control line parameters (p_2 and p_3) and compares the difference between modifying the inboard versus the outboard. Five designs (each having a different set of curvature definition parameters) were chosen from the previous study (#4), when the control line parameters were the same as the baseline's, $p_2=p_3=0.5$. These chosen designs were then modified using various control line parameters. The values used for each of the parameters modified in this study are shown in Table 8. A total of 80 ($4 \times 4 \times 5$) permutations were possible. Figure 12 shows the weight and flutter results plotted twice, i.e., both subplots show the same data but the symbols are sorted differently. The solid triangles indicate the designs chosen from the previous study. The symbols located around each solid triangle are the results of varying the control line parameters. In Figure 12(a), the data is sorted by control line parameters in the inboard wing section, and in Figure 12(b), the data is sorted by control line parameters in the outboard wing section.

Table 8. Study 5: stringer control line and OBD and IBD sensitivities, $p_1^* = [00000000]$.

	Modified parameters	Parameter values
Control line of IBD	p_{2_i}, p_{3_i}	[0.2, 0.2], [0.8, 0.8], [0.9, 0.1], or [0.1, 0.9]
Control line of OBD	p_{2_o}, p_{3_o}	[0.2, 0.2], [0.8, 0.8], [0.9, 0.1], or [0.1, 0.9]
Curvature definitions of 5 designs from previous study which uses [0.5,0.5] for the control line	$p_{4_i}, p_{5_i}, p_{6_i}, p_{5_o}, p_{6_o}$	[4, 0.25, 4, 4, 4], [1, 0.25, 4, 4, 4], [0.25, 1, 4, 4, 4], [1, 0.25, 0.25, 4, 1], or [4, 0.25, 4, 0.25, 0.25]

By comparing the two subplots, the designs having the same control line parameters in the outboard have similar flutter resistance, where changes to the inboard only seem to affect the weight of the design, not its flutter resistance. Therefore, as seen earlier, the wing's stability is most affected by the inertial distribution in the outboard portions of the wing. Additionally, the control line parameters of [0.9, 0.1] provide about a 3% increase in the flutter speed compared to the other control line parameters. Figure 13 defines the outboard curvature definition parameters, p_{6_i} , p_{5_o} , and p_{6_o} , as [4,4,4] and applies control line parameters [0.9, 0.1] (solid lines) and [0.1, 0.9] (dashed lines) to compare the resulting difference in the stringer shapes. The stringers having the [0.9, 0.1] control line parameters bend toward the leading edge in the midsection of the outboard wing, where the stringers having the [0.1, 0.9] control line parameters are more aft. Considering that a similar improvement could be made by updating the control line in the curvilinear spar designs of studies #2 and #3, the best design in study #3 (the upper leftmost design in Figure 10 (b)) was modified to have [0.9, 0.1] as its control line parameters for the outboard wing section. The resulting flutter speed was increased by 2.1%.

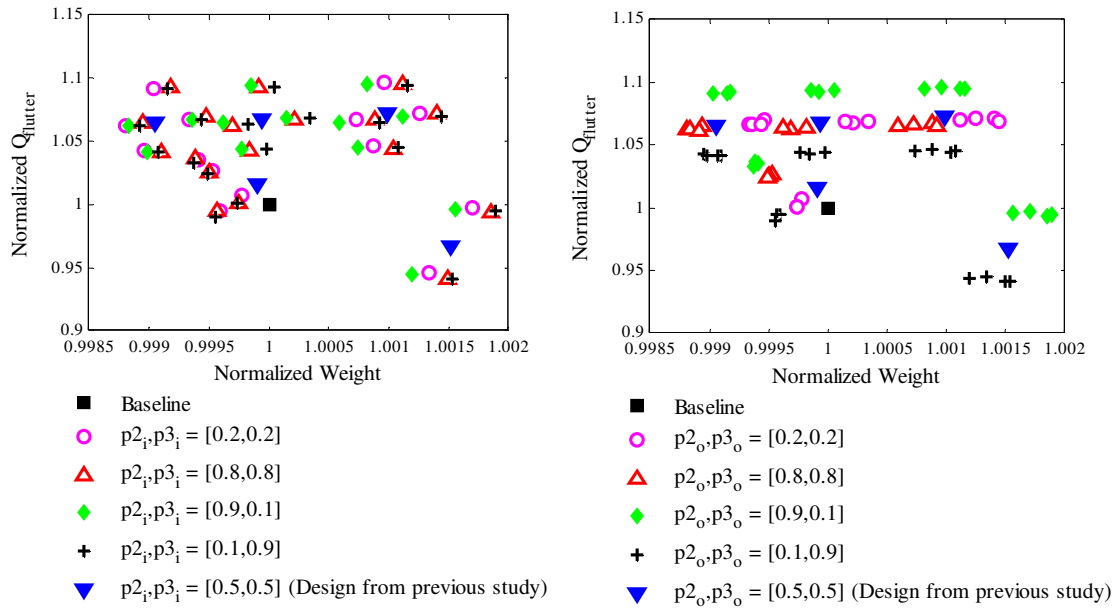


Figure 12. Results of the stringer curvature study when the control line position is different between the IBD and OBD wing sections (study #5).

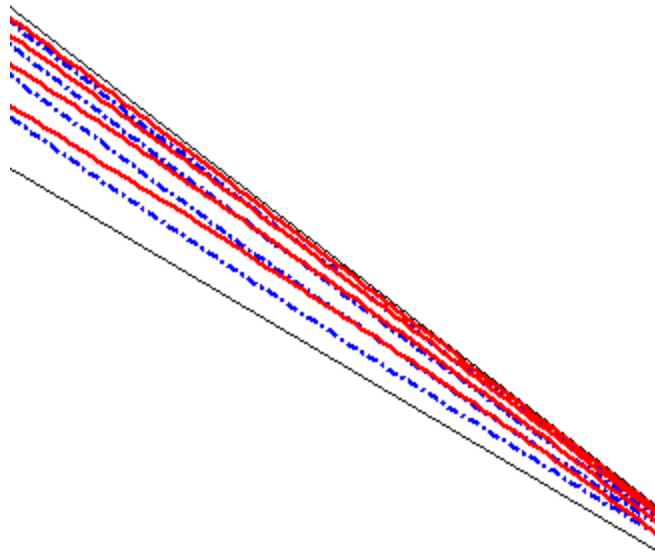


Figure 13. Comparing the stringer curvature resulting from control line parameter values of [0.9, 0.1] (solid lines) and [0.1, 0.9] (dashed lines) within the outboard wing section of the parameterized model, where the curvature definition parameters $[p6_i, p5_o, p6_o]$ equal [4, 4, 4].

V. Rib Topology Studies

Six parametric studies are conducted to evaluate the effect of various rib topologies. The first two studies involve straight ribs: the number of ribs and their orientation. The remaining studies consider the effects of rib

curvature. It is important to keep in mind that one role of the ribs is to preserve the airfoil shape (the outer mold line) under air loads [14], making their spacing (topology) significant. The analysis here does not capture this role.

A. Number and Location of Straight Ribs

The first parametric study of the ribs (study #6) explores the effect of the number of ribs on the wing weight and flutter speed. The values used for each parameter are described in Table 9. Figure 14 summarizes the results of analyzing all combinations of the number of ribs in the inboard and outboard sections and compares them to the baseline design, which has 10 ribs in the inboard section and 25 ribs in the outboard section. The two arrows in the figure show the trends when increasing the number of ribs in both the inboard and outboard wing sections. The slopes of these arrows clearly show that increasing the number of ribs in the outboard section has a larger effect on the wing's stability than increasing the number of ribs in the inboard section. This is because straight ribs do not bear as much load (as a spar would for example) so their main impact here is inertial, where inertial changes in the outboard affect flutter speed the most [13]. Interestingly, when compared to the baseline, designs with fewer ribs in the inboard and more ribs in the outboard can have both lighter weight and an increase in flutter speed; however, these designs may have buckling issues and/or may not sufficiently support the wing skin, at least in the inboard.

Table 9. Study 6: number of ribs.

	Modified parameters	Parameter values
# of ribs in IBD	p_{1i}	3, 6, or 10
# of ribs in OBD	p_{1o}	5, 10, 15, 20, 25, 30, or 35

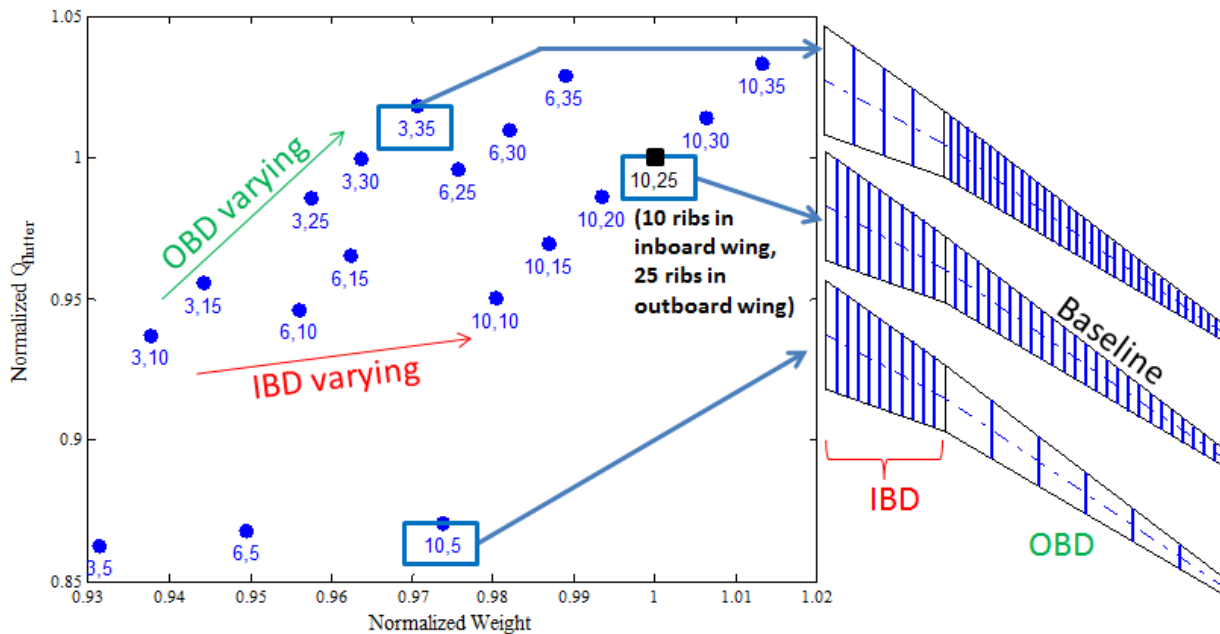


Figure 14. Results of the study on the number of straight ribs (study #6).

B. Orientation of Straight Ribs

The next parametric study (#7) explores the effect of the orientation of straight ribs. The values used for each parameter are described in Table 10. Parameter p_7 is the angle of orientation of the straight ribs in degrees. Figure 15 shows the results compared to the baseline design. In this case, no design was superior to the baseline (meaning no design had both less weight and a higher flutter speed). The results indicate a clear trend, however, with both a maximum and minimum flutter speed (this same trend is found in [7].) The maximum flutter speed occurs when the rib orientations are at 24 degrees, labeled as 'a'; the minimum flutter speed occurs when the rib orientation are at -36 degrees, labeled as 'b'. Although each design has the same number of ribs, the wing sweep causes the weight to vary between designs since the ribs become either longer or shorter based on their orientation within the sweptback

wing. The lightest configuration occurs when the ribs are normal to the leading edge, and therefore is commonly used in transport aircraft design [14].

Table 10. Study 7: rib orientation (IBD and OBD the same).

	Modified parameters	Parameter values
Rib orientation	$p7_i$ and $p7_o$ ($p7_i = p7_o$)	Various values chosen between -57 and 30 degrees. Designs with values above 30 had difficulties meshing appropriately and could not be evaluated.

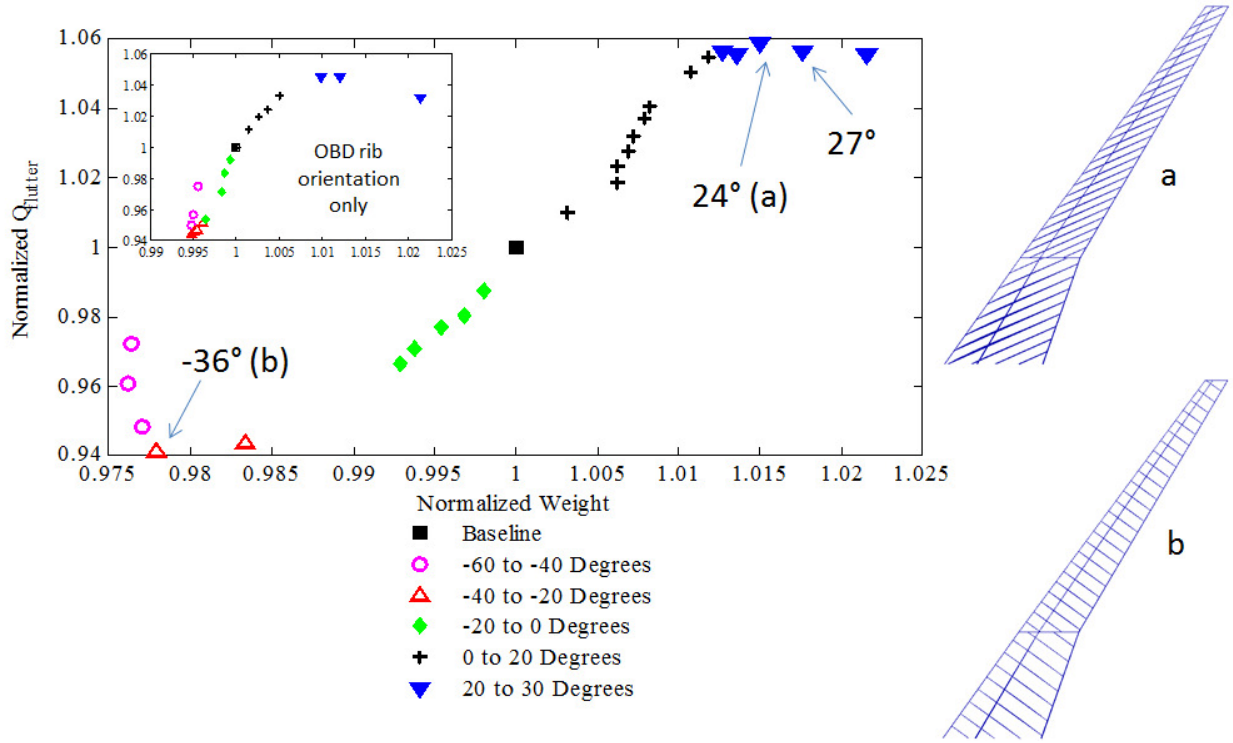


Figure 15. Results of the straight rib orientation study (study #7 [and study #8]).

The next parametric study (#8) only explores the orientation of the outboard ribs; the inboard ribs are straight and parallel with the flow, just like the baseline. The values used for each parameter are shown in Table 11. The subfigure of Figure 15 shows that the trend continues to hold, although there is a slight decrease in flutter resistance and weight range, as compared to study #7 when the inboard ribs are also reoriented.

Table 11. Study 8: rib orientation (IBD and OBD different).

	Modified parameters	Parameter values
Rib orientation	$p7_o$	Various values chosen between -58 and 34 degrees. Designs with values below -58 and above 34 had difficulties meshing appropriately and could not be evaluated.

C. Rib curvature

The next three parametric studies (#9, #10, and #11) investigate the effects of rib curvature. For the first study, the curvature definition parameters ($p4$, $p5$, and $p6$) are all assigned one of three values, 0.25, 1, or 4, resulting in 27 permutations. The control line location is also varied by changing $p2$ and $p3$ with the values shown in Table 12. When the three curvature definition parameters have the same value ($p4=p5=p6$), the ribs are straight although their spacing is not necessarily uniform depending on their value. Some examples were shown earlier in Figure 5. Figure

7 showed the effect when parameters p4-p6 were not equal. Various curvatures can be defined. The location of the maximum curvature can be modified by the values of p2 and p3 which determine the control line position.

Table 12. Study 9: rib curvature (IBD and OBD rib parameters the same).

	Modified parameters	Parameter values
Control line	p2, p3	[0.5, 0.5], [0.2, 0.2], [0.8, 0.8], [0.9, 0.1], or [0.1, 0.9]
Curvature definition	p4, p5, p6	0.25, 1, or 4

These 27 permutations were first evaluated with the control lines used for the baseline, $p_2=p_3=0.5$. The results of these designs are indicated with symbols (as opposed to small dots) in Figure 16. The remaining designs, indicated by small dots, are the 27 permutations evaluated with the remaining four sets of control line parameters found in Table 12, resulting in 135 (27x5) maximum possible number of permutations. The design with the lowest weight is understandably the design with straight ribs all shifted outboard, where the wing taper decreases the volume of available material. Of all the designs, only a few were more superior to the baseline in terms of both the weight and flutter speed. Of these few designs, the design with the highest flutter speed is indicated by a star in the figure. This design is only slightly lighter (<0.2%) than the baseline design and has a 3.4% increase in flutter speed. The stresses also increased by 1.2% with respect to the KS function, which indicates increased aeroelastic stress levels throughout the wing.

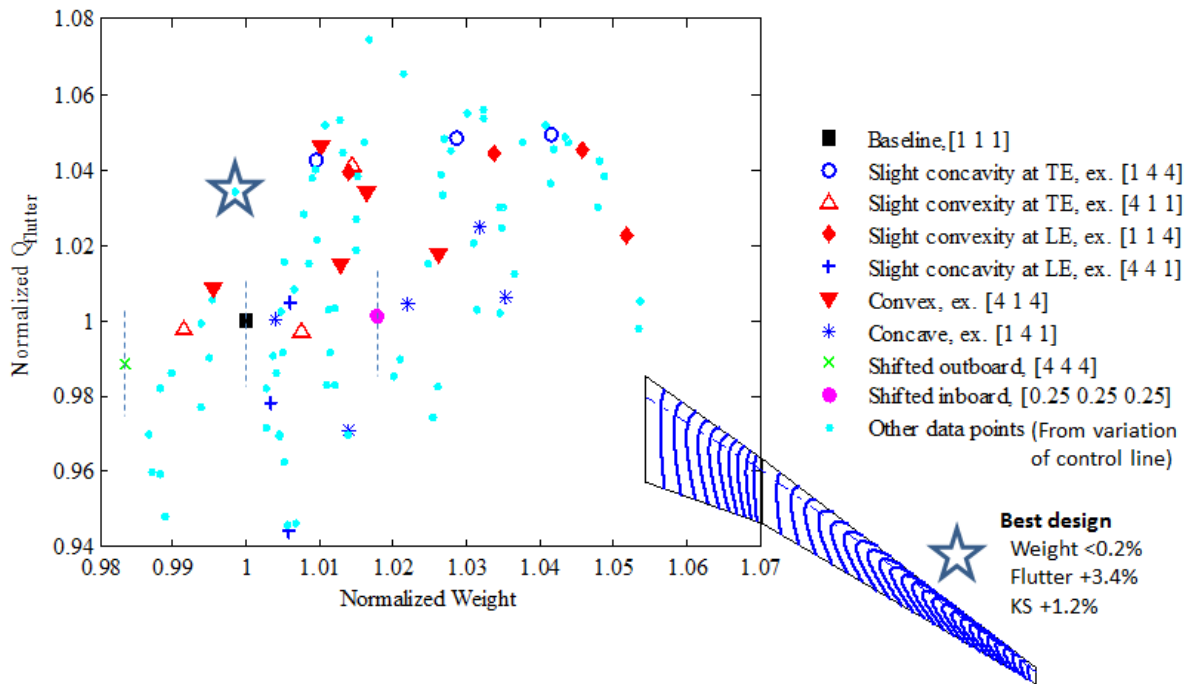


Figure 16. Results of the rib curvature study (study #9).

Looking at only the 27 original designs, there is one convex design that is slightly better than the baseline in both weight and flutter speed, but no trends are apparent based on convexity or concavity. Therefore, individual designs of the 27 original designs were compared to their counterpart designs that had the same curvature definition values (p4-p6) but different control line parameters (p2, p3). Figure 17 shows four sets of designs; designs (a) and (b) both have convex ribs, while designs (c) and (d) both have concave ribs. Each set of designs is sorted from best to worst in terms of flutter resistance. By observing the changes in the control line values from one design to another, the designs with convex ribs (a and b) have an increased flutter speed as the control line is shifted toward the *leading edge*. Designs (c) and (d) both have concave ribs and an increased flutter speed as the control line is shifted toward the *trailing edge*.

Interestingly, in all four groups of designs (a-d), those with the highest flutter speed (the leftmost designs) have a majority of their rib length at approximately 26 degrees orientation. This is similar to the results of the straight rib rotation studies (Figure 10) that had 24 degrees as the best rib orientation. In essence, the best curvature approximates the best rib rotation angle for the majority of the rib length. For comparison purposes, Figure 18 plots the results of these five designs, i.e. the best rib rotation design (from study #7) and the best flutter designs shown on the left side of Figure 17. Of the five designs, the design with ribs that are straight has the second highest flutter speed and the highest stress levels (represented by the KS function). All of the designs have a higher flutter speed than the baseline.

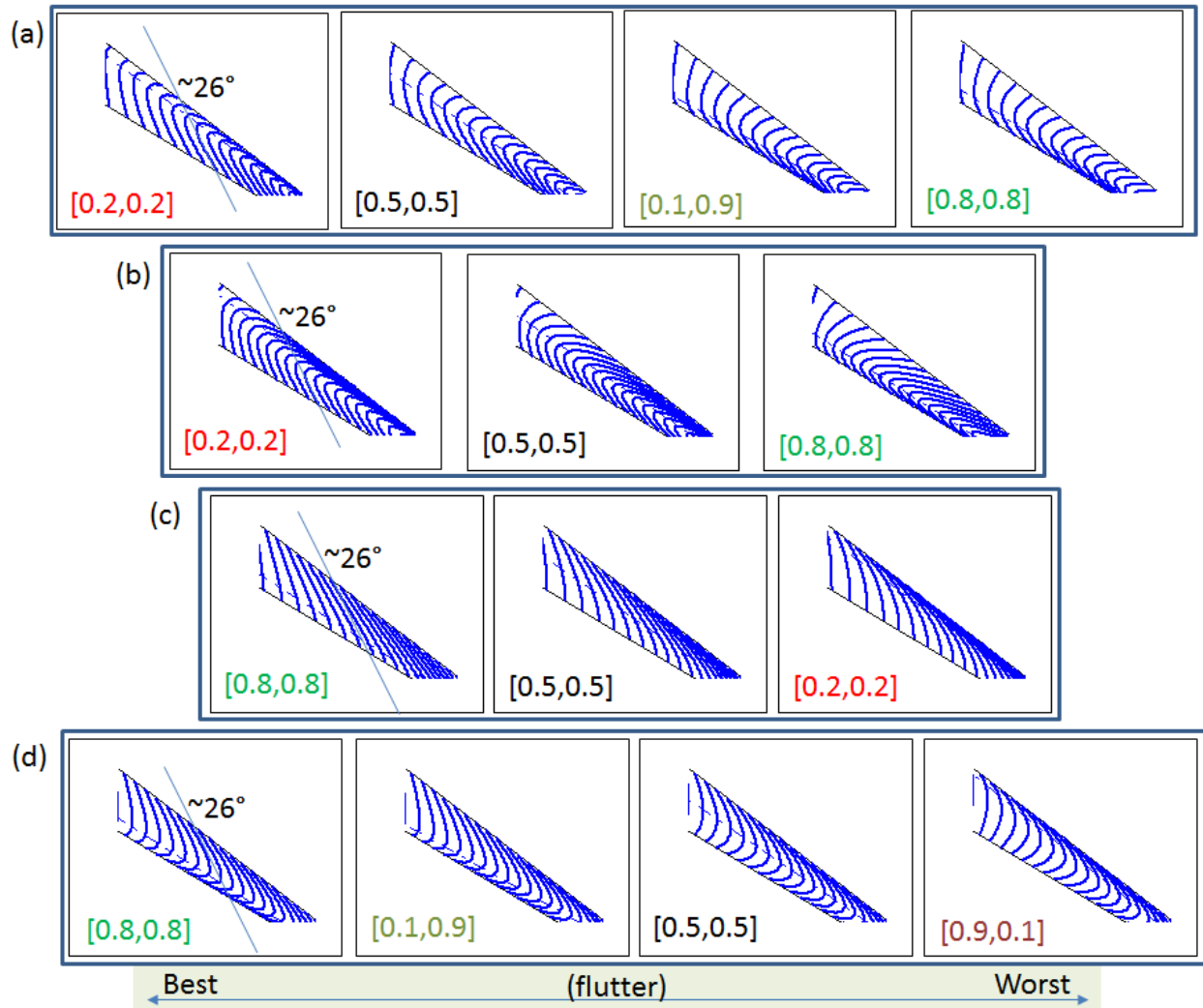


Figure 17. Comparison between four different groups of designs that each have the same curvature definition parameters (p4-p6) but differing control line parameters (p2,p3). The parameters p4-p6 are: (a) [4 1 4], (b) [4 0.25 1], (c) [1 4 4], and (d) [1 4 1]. The designs with the highest flutter speed are the left-most designs and all have their ribs oriented in a similar direction.

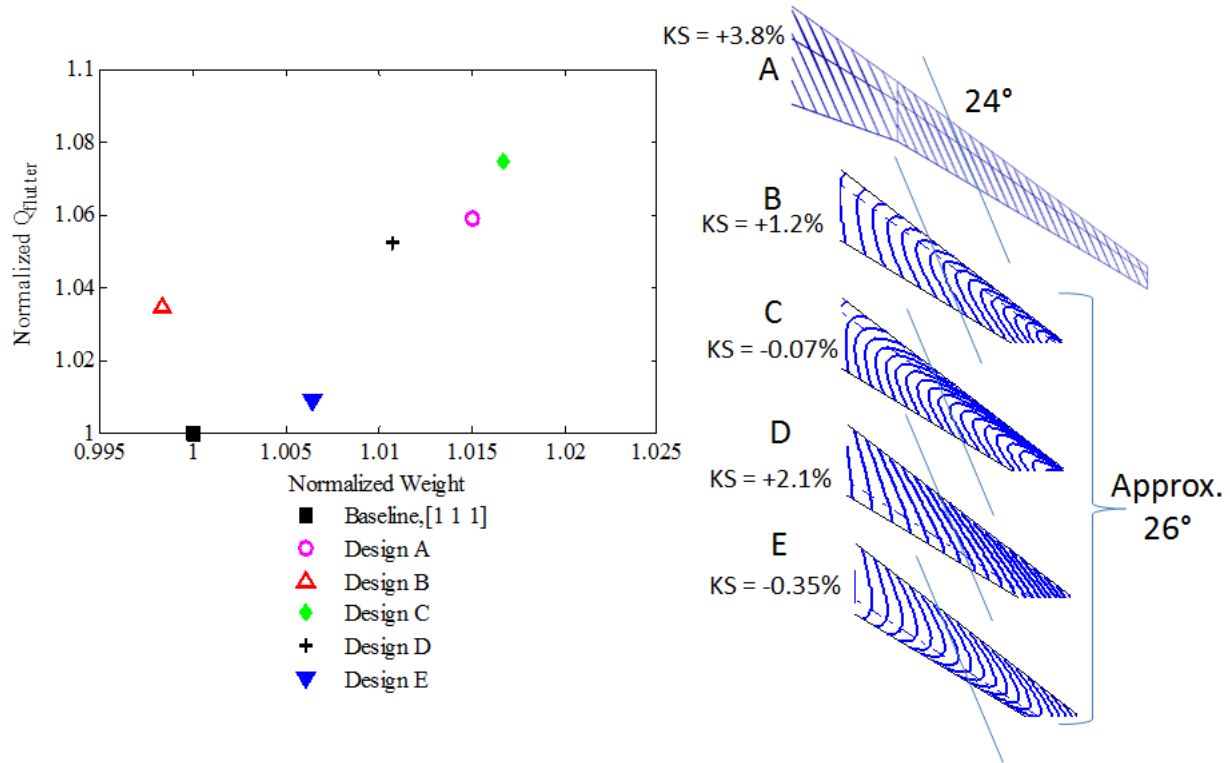


Figure 18. Comparing the best designs in the previous figure to the design in study #7 that has straight ribs all oriented at 24 degrees.

The next parametric study (#10) removes the spar to determine whether the trends of the previous study are dependent on the presence of the inner spar. The same set of 27 permutations of curvature definition parameters (p4-p6) were used. Permutations of the three sets of control line parameters are shown in Table 13 and define control lines at constant chord locations. A total of 81 (27x3) permutations were possible. Figure 19 compares the results from designs having no inner spar to the designs with a spar. The arrows in the figure identify corresponding designs that have the same rib configurations but either the absence or presence of an inner spar. With the absence of the spar, the flutter speed decreased by 2-8%. This range in flutter penalties indicates that some rib designs are less sensitive to spar removal than others, meaning that they potentially make up for the lost stiffness and mass of the missing inner spar.

To investigate why some rib configurations may have a lower flutter penalty, Figure 20 plots each rib design by its flutter penalty versus its normalized weight. A general, linear trend is apparent, suggesting that heavier designs will have a larger decrease in flutter speed when the inner spar is removed, which seems counterintuitive. For designs having the same weight, the data still shows about a 3% range in flutter penalty values. Therefore, for the same weight, some rib configurations are less sensitive to the spar removal than others. To explore this, Figure 21(a) shows designs least affected by spar removal, with respect to weight (i.e., these five designs are located on the lower edge of the band of points in Figure 20 and are circled). Figure 21(b) shows designs most affected by spar removal, with respect to weight (i.e., these five designs are located on the upper edge of the band of points in Figure 20 and are also circled). The designs in Figure 21(a) have greater curvature than designs in Figure 21(b), suggesting that designs having more rib curvature partially serve as the missing spar.

Four designs are highlighted in Figure 20: two designs have maximum curvature near the spar location, a third design has maximum curvature near the trailing edge, and a fourth design has rotated straight-ribs (this design was the best design of the rotated rib study and was added for comparison purposes). Since the inner spar is located toward the leading edge, it would be expected that designs having maximum curvature near the leading edge may be partially serving as a spar and have less of a flutter penalty. However, Figure 20 shows that a design having maximum curvature near the trailing edge has comparable flutter penalties with those designs having maximum curvature near the inner spar location, especially when taking into account the linear trend across the data.

As a final observation, three of the four designs illustrated in Figure 20 have nearly the same weight. As expected, the design with no rib curvature has the greatest flutter penalty. The other two designs have ribs of similar curvature and lower penalties, yet there is a relatively large discrepancy between their flutter penalties, indicating again that the location of maximum curvature is not a clear indicator of a design's flutter resistance in the absence of an inner spar. However, in general, these initial studies suggest that for the same weight, designs that have more rib curvature tend to have less of a flutter penalty when the inner spar is removed.

Interestingly, the new results in Figure 19 indicate a design more superior than the best design in the previous rib study, at least with respect to weight and flutter speed. Originally, when this particular rib design had a spar, it had about a 7% higher flutter speed than the baseline but was heavier than the baseline. With the removal of the spar, the weight is now 5.5% less than the baseline and the flutter speed is now 5.1% higher than the baseline. The stresses however increased by 2.9% with respect to the baseline's KS value.

Table 13. Study 10: rib curvature without the inner spar included (IBD and OBD rib parameters the same).

	Modified parameters	Parameter values
Control line	p2, p3	[0.5, 0.5], [0.2, 0.2], [0.8, 0.8]
Curvature definition	p4, p5, and p6	0.25, 1, or 4

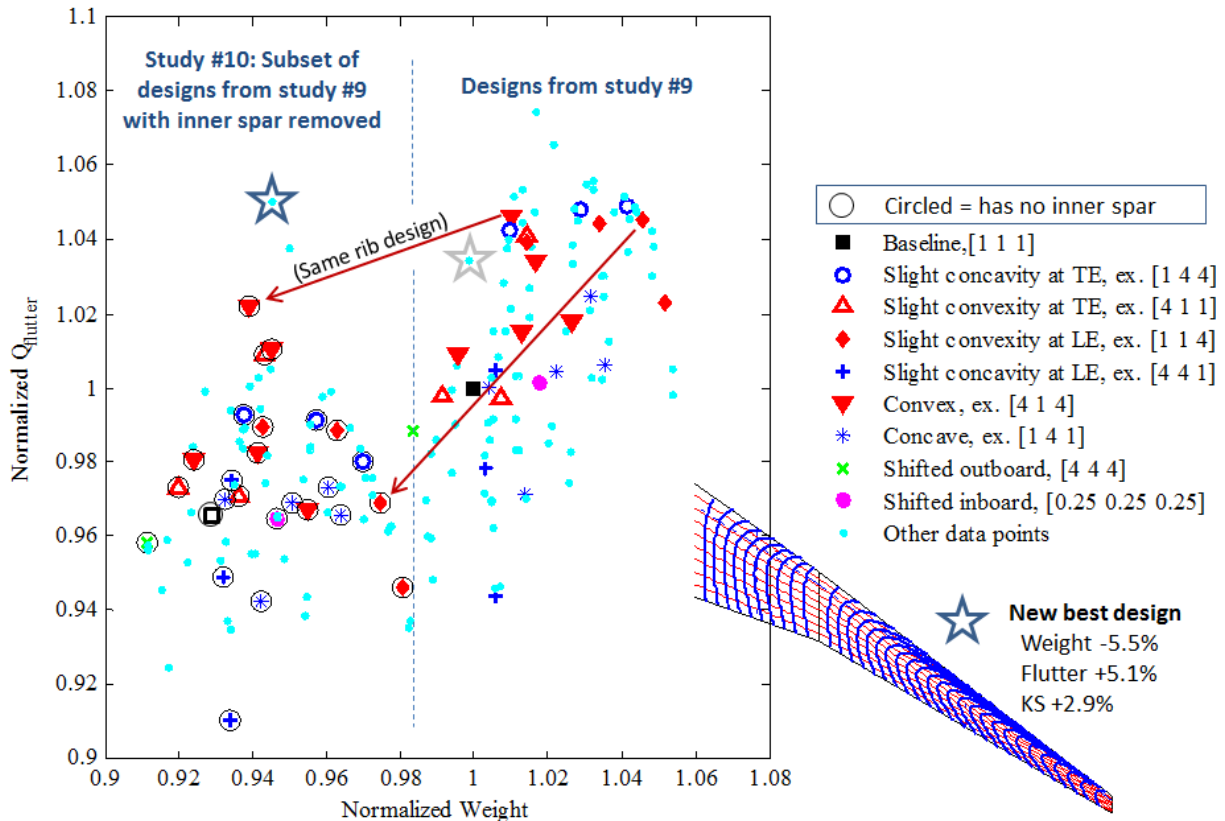


Figure 19. Results from the rib curvature study having no inner spar (study #10).

The third parametric study involving curved ribs (study #11) employs different rib curvatures for the inboard and outboard wing sections. Table 14 shows the parameters varied in this study; the control line variable in the inboard and outboard sections were limited to either [0.2, 0.2] or [0.8, 0.8]. In addition to these parameters of Table 14, an additional case with straight ribs was considered, where the parameters for p2-p6 were [0.2, 0.2, 1, 1, 1]. Figure 22 summarizes the results for this study. Figure 22(a) and (b) both show the exact same data; however, the data is sorted differently between the two figures. Referencing Figure 22(b), only half of the designs are highlighted

with symbols as opposed to small dots. These designs were selected for clarity purposes and all have [0.8, 0.8] as the control line parameters in the outboard section of the wing. Their symbols distinguish which curvature definition parameters each design has in the outboard wing section. These same designs are highlighted in Figure 22(a), but their data points are now sorted by the curvature definition parameters (p4-p6) within the inboard section of each wing design. Figure 22(b) shows how the designs having the same curvature definitions in the outboard all have nearly the same flutter speed, while Figure 22(a) shows that the inboard curvature definitions of these designs tends to affect the weight of a design but not its flutter speed. Once again, changes to the outboard have a greater effect on the wing's aeroelastic response, than the inboard.

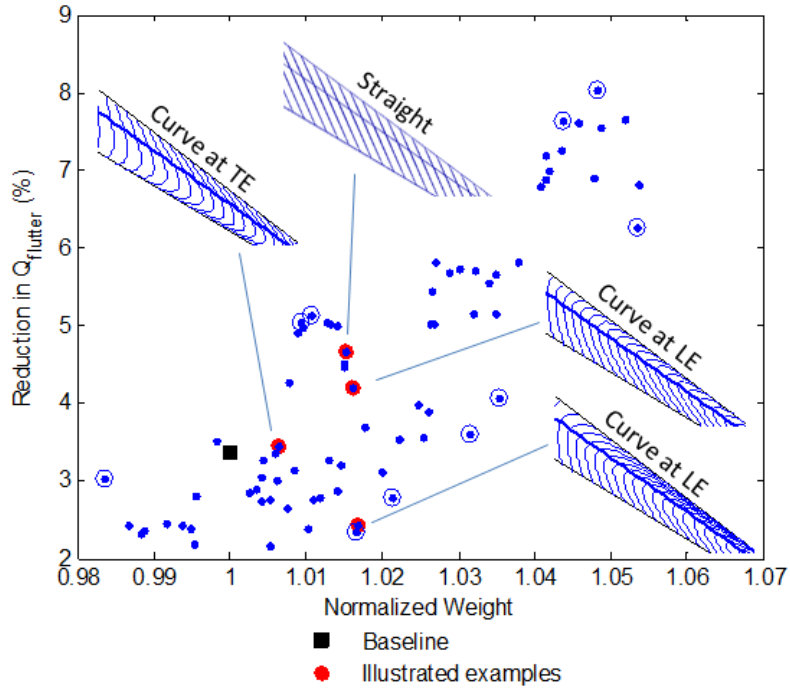


Figure 20. The reduction of flutter speed due to removal of the inner spar (study #10).

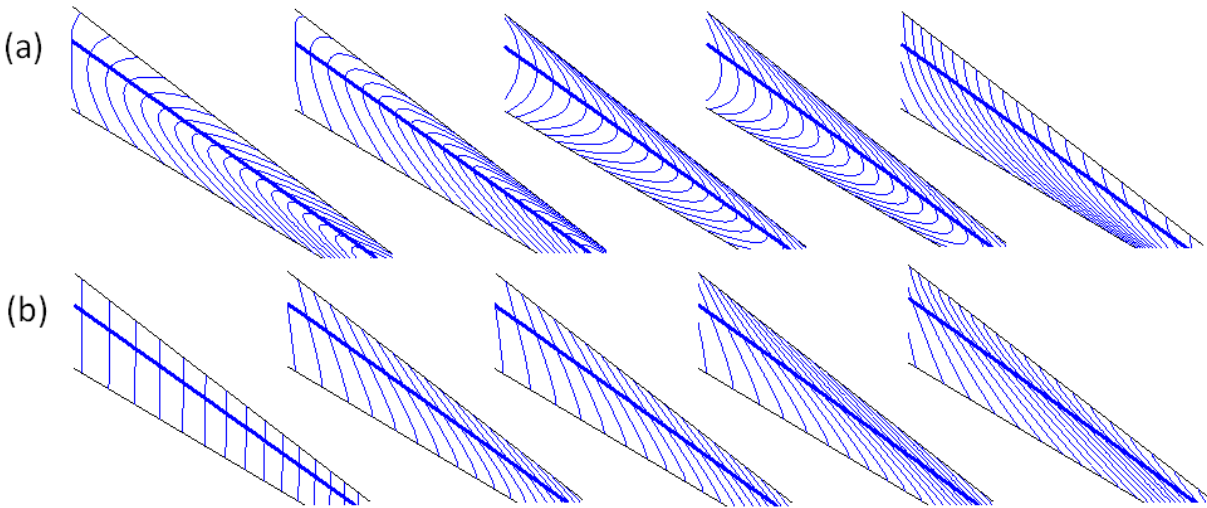


Figure 21. Designs corresponding to the circled data points on the upper (b) and lower (a) edges of the band in Figure 20.

Table 14. Study 11: rib curvature (IBD and OBD rib parameters different).

	Modified parameters	Parameter values
Control line	p2, p3	[0.2, 0.2] or [0.8, 0.8]
Curvature definition	p4, p5, and p6	[4, 0.25, 1], [4, 1, 4], [1, 4, 4], or [0.25, 4, 1]

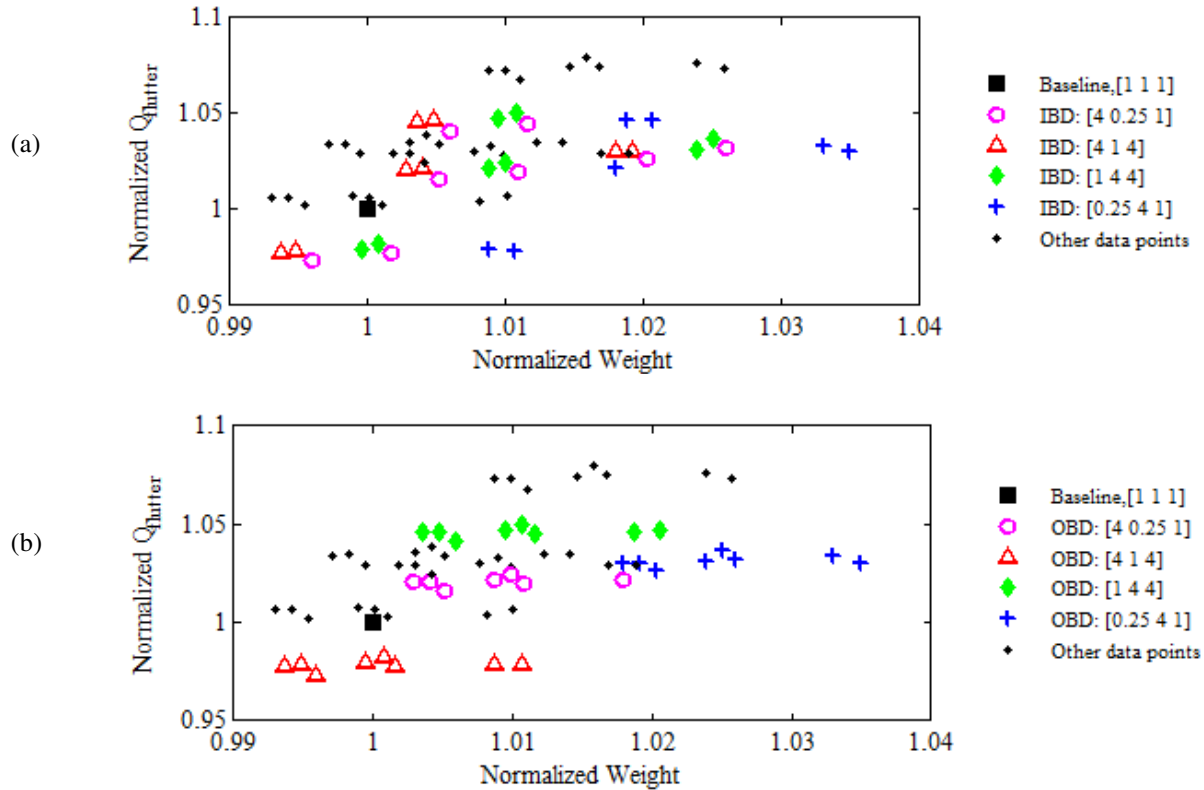


Figure 22. Results of the rib curvature study which uses different rib definitions between the IBD and OBD wing sections (study #11).

VI. Combining Curvilinear Spars and Ribs

To this point, the effect of having curvilinear spars, ribs, and stiffeners simultaneously has not been explored; however, given a few of the studies above which removed spars from a design, there is indication that changes to spars or ribs may be fairly independent of one another. This section provides one parametric study that combines curvilinear spars, stringers, and ribs, where the results here are less thorough than before since the design space is larger.

In this study, curvilinear spars and curvilinear ribs are combined to determine whether their relative performances complement (create a more superior design) or oppose one another. The 27 rib permutations from study #9 (which all used straight spars) are used for the comparison. For each of the rib permutations, three new designs were created, each using a different curvilinear spar definition, creating at most 108 (27+27x3) design permutations. These new designs were then compared back to the original rib permutation having straight spars. Figure 23 shows the three alternate spar configurations chosen ‘a’ - ‘c’, and Table 15 shows the values of each parameter modified. Each of the three designs have different values for their outboard-most control points, p_{5_o} and p_{6_o} , where p_{5_o} was constrained to equal p_{6_o} . This choice of parameters was based on the results of studies #2 and #3, to ensure a large range of flutter speeds between the three spar designs. It was more important to have spar designs with a range of flutter speeds than to have spars that were curvilinear along their entire span, since the flutter resistance of each spar/rib combined design is evaluated here for trends.

The results of this study are shown in Figure 24. The permutations using design ‘a’ for the spar configuration are highlighted with circles. The permutations using design ‘c’ are highlighted with triangles. The permutations using $p_{5_o} = p_{6_o} = 1$ (design ‘b’ and the straight spars) are highlighted with squares and indicated in the figure. In the figure, five groups of designs are identified, where each group has a constant rib configuration. The trend is consistent between each group of designs, suggesting that independent of the rib configuration, a design can have an increase in its flutter resistance by incorporating a spar configuration that is of higher performance than its current

configuration. The next section of the paper is focused on trends in the data and will continue to explore whether rib and spar configurations that have a high resistance to flutter continue to complement one another when combined.

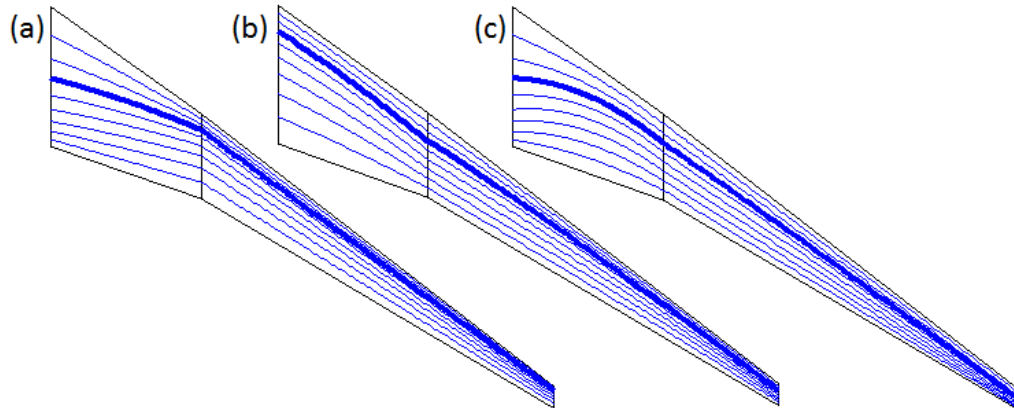


Figure 23. Three curvilinear spar/stringer configurations applied to the 27 original curved rib designs from study #9.

Table 15. Study 12: combined curvilinear spars and ribs.

	Modified parameters	Parameter values
Rib curvature definition (creates 27 permutations)	p4, p5, and p6	0.25, 1, or 4
Spar definition	[p2 _i , p3 _i , p2 _o , p3 _o , ... p4 _i , p5 _i , p6 _i , p5 _o , p6 _o]	Spar/stringers(baseline): [0.5,0.5,0.5,0.5,1,1,1,1,1]; Spar/stringers(a): [0.5,0.5,0.5,0.5,0.25,1,4,4,4], Spar/stringers(b): [0.5,0.5,0.9,0.1,4,4,1,1,1], or Spar/stringers(c): [0.5,0.5,0.9,0.1,0.25,4,1,0.25,0.25]

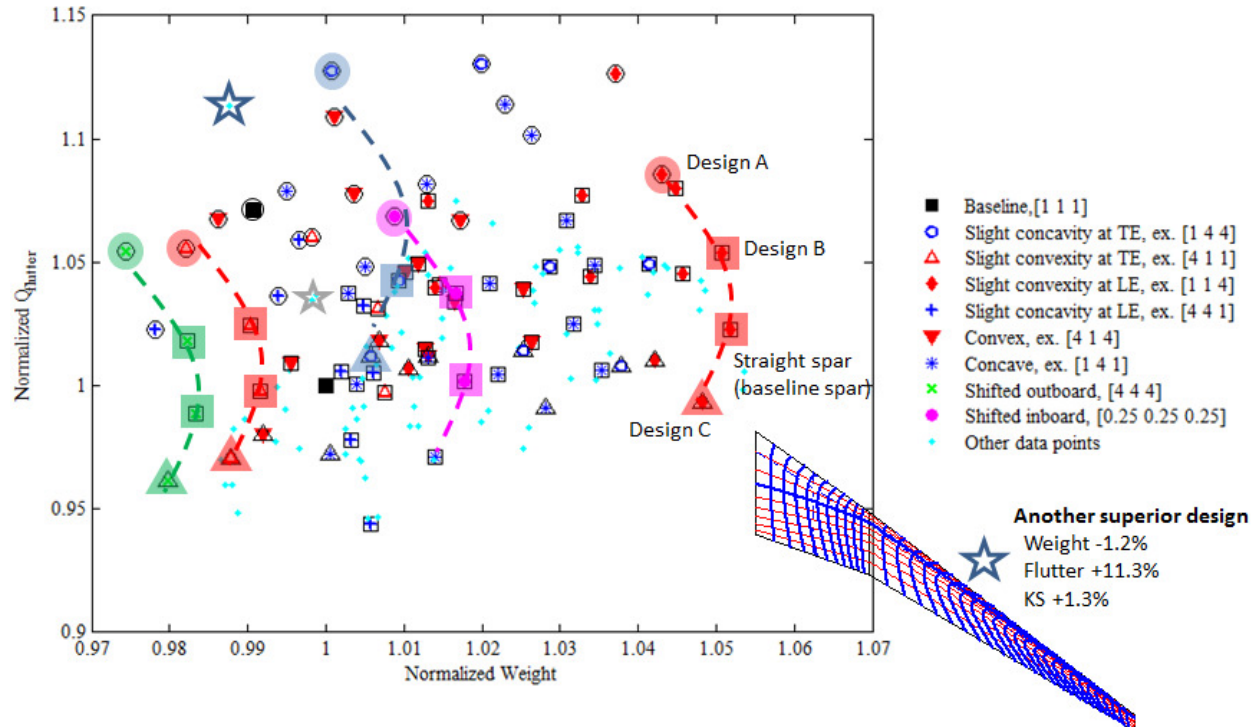


Figure 24. Results from combining curvilinear spars with curvilinear ribs (study #12).

Given this trend, the best design of the previous rib curvature study shown in Figure 16 was modified to have a high performing curvilinear spar, which used the parameters of design ‘a’ except for (p_{2o} and p_{3o}) which were updated to be [0.9, 0.1] (the highest performing control line for spars). This design is illustrated in Figure 24. The result is a 1.2% decrease in weight and an 11.3% increase in flutter resistance. The stresses also increased by 1.3% with respect to the KS function. Thus, by comparing this design with the best design in Figure 19, which had rib curvature and no spar, this design outperforms in flutter resistance but not in weight reduction.

VII. Identifying Design Trends

The goal in this section is to identify design trends that lead to lighter-weight, aeroelastically stable wing designs, with respect to the baseline. Weight and flutter were the focus of the previous parametric studies (#1-12). As mentioned earlier, other evaluation metrics were calculated for each design, including: an aggregate stress function (the Kreisselmeier-Steinhauser (KS) function), the position of the wing’s flexural axis (measured at the wing tip), the global buckling eigenvalue, the wing tip deflection, the wing tip twist, the shear at the root, the root bending moment, the root torsional moment, and the center of gravity (CG) of the wing. Additionally, the CG of eight individual spanwise segments of the wingspan was calculated so that the section CG at the root (CG_{root}) and the section CG at the wing tip (CG_{tip}) could be evaluated for variances in mass distribution along the wingspan. These evaluation metrics are considered in this trend-identification study to provide additional insight into each wing’s properties and behavior.

Given the many design perturbations generated over the twelve parametric studies, only a subset of those designs are analyzed for trends. Multiple subsets (referred to as groups) were chosen to observe whether a trend is consistent across all groups of designs. Table 16 provides information about each of the groups (A-G). In all cases, except group G, the designs chosen for the group came from a single parametric study. Since some studies did not have much weight variation amongst the designs, due to keeping the number of structural members (spars and ribs) constant for comparison purposes, designs having a large range in flutter speeds and similar weight were chosen for each group.

Groups A and B had the smallest range in weight because they were chosen from studies that only varied the curvature of the spars or stringers. Groups C – E had slightly larger changes in weight; however, these designs were

specifically chosen from parametric studies that only varied a single parameter, such as the spar location study (where spanwise members were toggled between spars and stringers using $p1^*$ in Figure 9) or the rib orientation studies (where the straight ribs were rotated by $p7$ in Figure 15). This way, the change from one design to another was gradual and intentional such that potential trends may be easier to detect. For example, in group D, which uses designs that varied the location of two spars, only four designs of a possible twelve were chosen for the subset. These designs placed a pair of adjacent spars in four different locations from leading edge to trailing edge, i.e. $p1^* = [11000000], [00110000], [00001100],$ and $[00000111]$.

Group F has the broadest range in flutter speeds. Unlike the previous three groups, this group does not have a small change in its internal structure configuration from one design to the next since the designs were chosen from the study that combined the curvilinear ribs and curvilinear spars, resulting in multiple parameters changing from one design to the next. Finally, the designs chosen for group G were taken from the best designs across multiple studies. All of the designs within this group have a lower weight and higher flutter speed than the baseline. The purpose of this group is to detect whether these designs all have something in common that can explain their superiority to the baseline with respect to weight and flutter speed.

Table 16. Description of groups of designs used for the trends study

Group ID	Group title	Studies (and corresponding figures) where the subsets of data were sourced	Weight range (%)	Flutter range (%)	Figure showing trend data
A	Spar/stringer curvature	Spar/stringer curvature #3, (Figure 10(b))	0.36	13.7	Figure 25
B	Stringer only curvature	Stringer curvature #4, (Figure 11)	0.07	12.3	Figure 26
C	Location of 1 spar	Spar number and location #1, (Figure 9)	2.1	6.0	Figure 27
D	Location of 2 spars	Spar number and location #1, (Figure 9)	3.3	10.6	Figure 28
E	Rib orientation	Rib orientation #7, (Figure 15)	3.9	11.7	Figure 29
F	Large flutter range	Combined curvilinear spars and ribs #13, (Figure 24)	0.72	18.2	Figure 30
G	Improved weight and flutter resistance	#2, #3, #4, #5, #6, #9, #10, and #12 (Numerous figures above)	7.4	12.9	Figure 31

Table 17 summarizes the most apparent trends observed from reviewing the data found in groups A – G. Data from each of the groups is organized in Figure 25 – Figure 31. Each figure has fifteen plots labeled (a) – (o). Since each group of designs has a relatively large range in flutter speeds, the normalized dynamic pressure at flutter is always used for the x-axis. When looking for correlations, the focus was more on detecting general trends and less on quantifying the correlations. For that reason, the y-axis of all the plots in these figures is also normalized; the title above each plot indicates the evaluation metric being considered.

The first trend involves weight and is observed in groups C - G. (Groups A – B did not have a large enough weight range to observe a trend). As weight was decreased in the wing, both the wing tip deflection and the stresses increased. As weight was increased, the two measurements decreased, recalling that a lower KS value indicates decreased aeroelastic stress levels throughout the wing. Since weight was not included as the x-axis in the plots, these observations were detected by comparing the profile of the weight vs. flutter speed plot (plots a) with the profiles of the tip deflection (plots e) and KS (plots b). For example, in group C, shown in Figure 27, the weight profile with respect to flutter speed in plot (a) resembles a rotated letter “C” and is similar yet inverted for both the tip deflection (plot e) and KS (plot b). This trend is not surprising and somewhat trivial, considering that the addition of weight would likely increase the wing’s stiffness, which would in turn decrease the tip deflection and subsequently result in less stress in the wing.

The next trend (#2) indicates a relationship between the wing weight and the location of the flexural axis. For example, this is noticeable in group C (Figure 27), since the flexural axis profile of plot (d) resembles the rotated “C”-shaped weight profile of plot (a). This trend is detected in groups C – E. This relationship must be an indirect

relationship (dependent on some other feature of the wing design) since the flexural axis is only affected by stiffness, not inertia.

The next two trends (#3 and #4) also involve the location of the flexural axis. These trends contradict one another, however. Trend #3 indicates more wash-out, as the flutter speed increases (and applies to groups A, C, and D), while Trend #4 indicates more wash-in, as the flutter speed increases (and applies to group E). Wash-out or wash-in is approximated here by the movement of the flexural axis (plots d) and the corresponding twist at the wing tip (plots h), where neither of these metrics is a true indicator of wash-in or wash-out but have shown correlations, especially when the inertial properties of the wing remain constant [10]. When the flexural axis moves forward, away from the swept wing, the moment arm between the flexural axis and the loads on the wing increases potentially causing more wash-out, which is consistent with the additional tip-down twisting of the wing. The opposite occurs with wash-in; the flexural axis typically moves aft with the wing tip twisting up. This trend for wash-out is clearest in group A, Figure 25 (plots d and h). Here the weight variation is extremely small, so unlike groups C – E where the weight profile was also observed in the flexural axis plot (as described by trend #2), the trend is not affected by the weight.

The inconsistency with wash-in and wash-out trends may be partially explained by considering the differences between the groups. Groups A, C, and D all indicate wash-out and have variability only in their spar and stringer designs. Group E indicates wash-in and has variability in the orientation of the ribs. Secondly, both wash-in and wash-out have been used in the literature to explain aeroelastic tailoring, but the wings referred to in those studies typically have a constant mass or constant mass distribution [10]. By keeping in mind that wash-in and wash-out are products of the wing’s stiffness distribution, they only partially affect the wing’s dynamics, as mass and its distribution also play a major role in stability.

By considering mass distribution, it is possible that the spars and stringers have an entirely different effect on the mass distribution than the ribs do. Therefore, the data was analyzed for trends involving the wing’s CG, CG_{root} , and CG_{tip} (plots j – o). The same groups observed to have trend #3 involving wash-out all show their wing CG and CG_{tip} moving forward as the flutter speed increases, as seen by trend #5. Group E did not indicate such a trend. Therefore, during these parametric studies, as permutations on the wing designs were made, both the mass and stiffness distributions changed, making it difficult to find design trends that show a consistent correlation with an increase in flutter speed. This is further confirmed by groups F and G, which had many design parameters changing from one design to the next, such that patterns and trends were not detectable except for trend #1. It is possible that more trends are included in this data, but only the most obvious are discussed here.

Table 17. Description of the trends discovered in the data and the design groups that reflect those trends.

Trend	Notional cause	Notional effect	Groups						
			A	B	C	D	E	F	G
1	Decrease in weight (plot a)	Increase in tip deflection (plot e) Increase in KS (plot b)	N/A	○	○	○	○	○	○
2	Decrease in weight (plot a)	Flexural axis forward (plot d)	N/A	○	○	○			
3	Flexural axis forward (plot d) (Wash-out)	Increase in negative twist (plot h) Increase in flutter speed (x-axis)	○		○	○			
4	Flexural axis aft (plot d) (Wash-in)	Decrease in negative twist (plot h) Increase in flutter speed (x-axis)					○		
5	CG shifts forward (plot j) CG_{tip} shifts forward (plot l)	Increase in flutter speed (x-axis)	○		○	○			

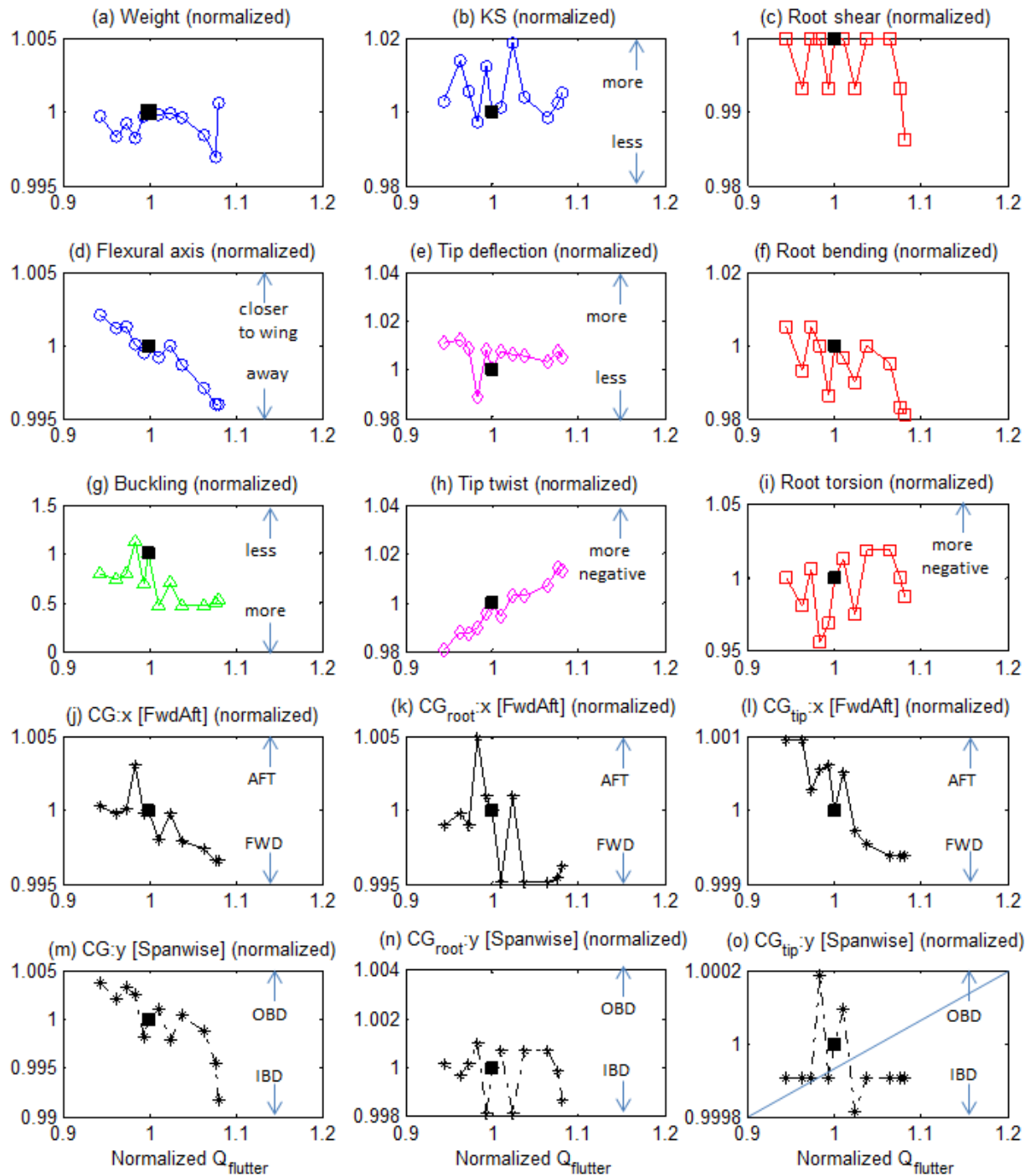


Figure 25. Data for group A (spar/stringer curvature). Plot crossed out has less than 0.1% range on the y-axis.

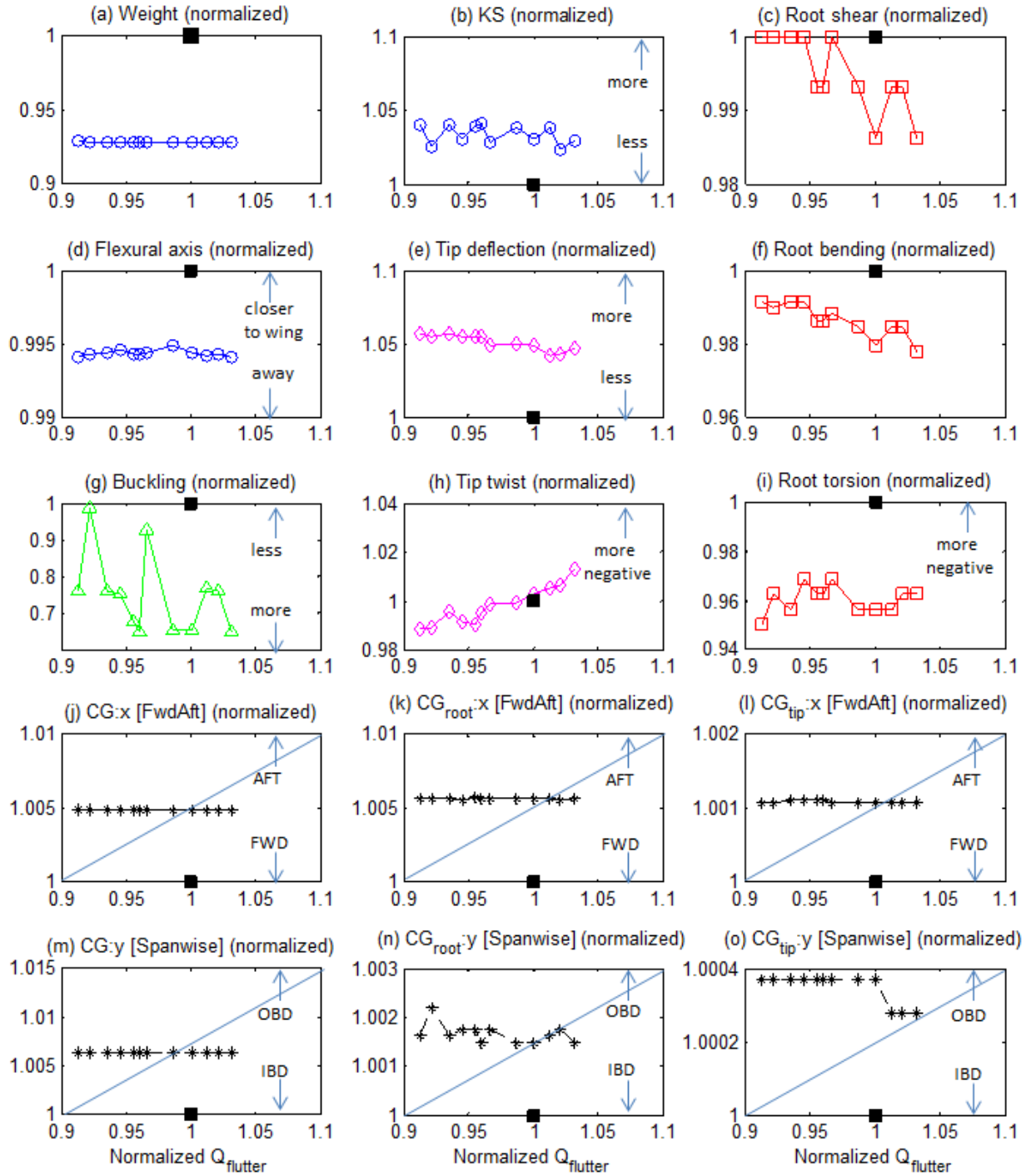


Figure 26. Data for group B (stringer only curvature). Plots crossed out have less than 0.1% range on the y-axis.

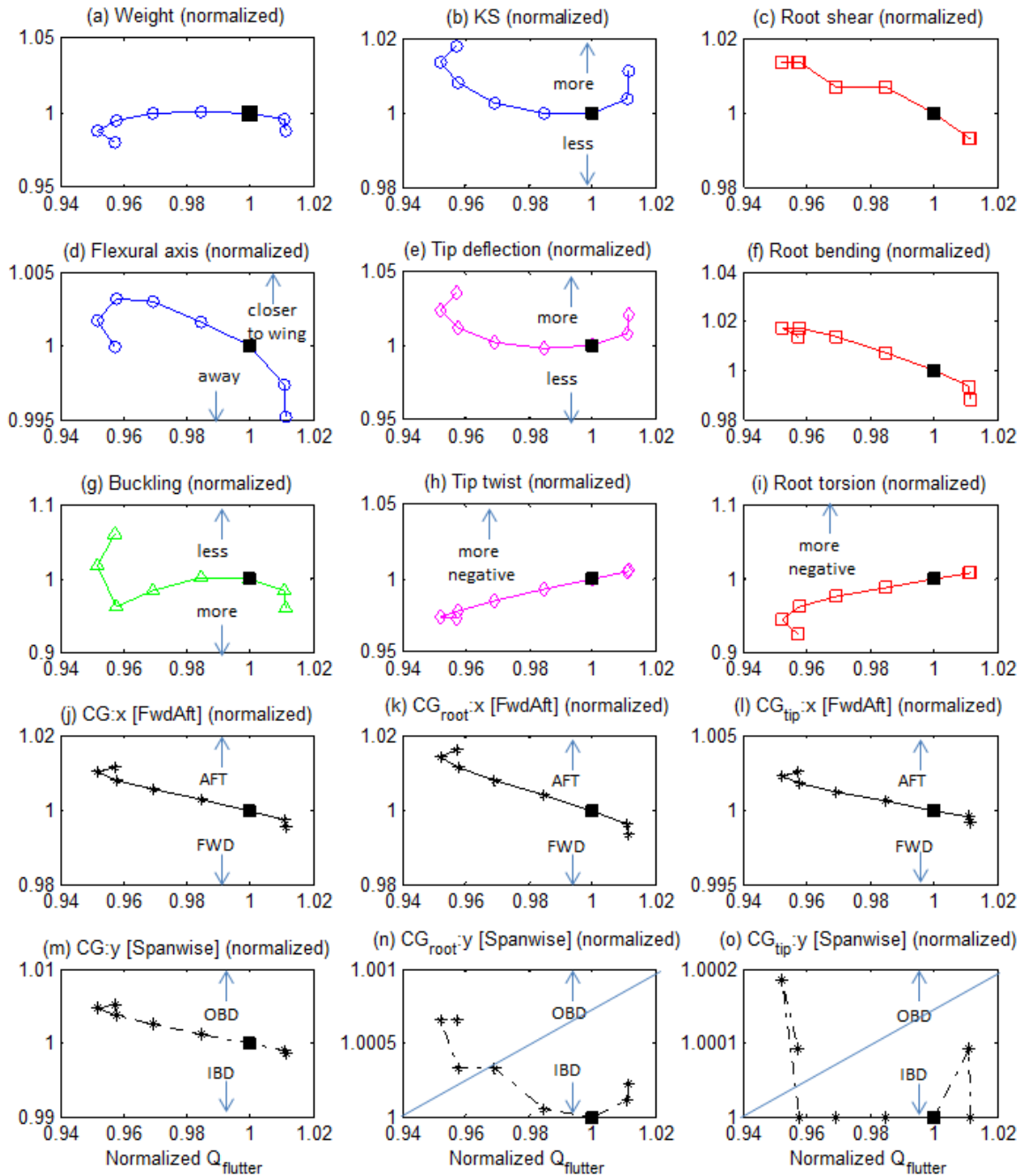


Figure 27. Data for group C (location of 1 spar). Plots crossed out have less than 0.1% range on the y-axis.

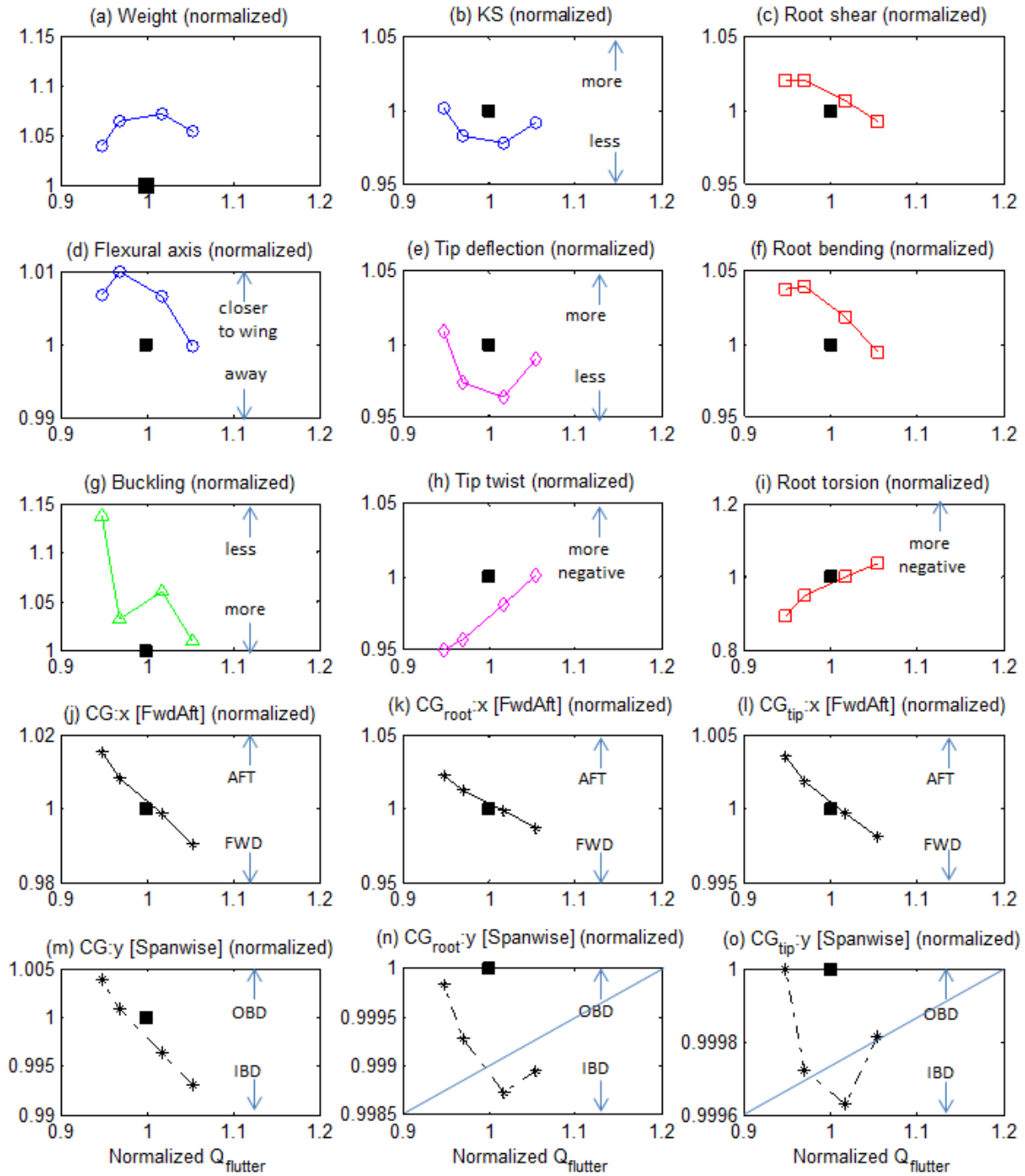


Figure 28. Data for group D (location of 2 spars). Plots crossed out have less than 0.1% range on the y-axis.

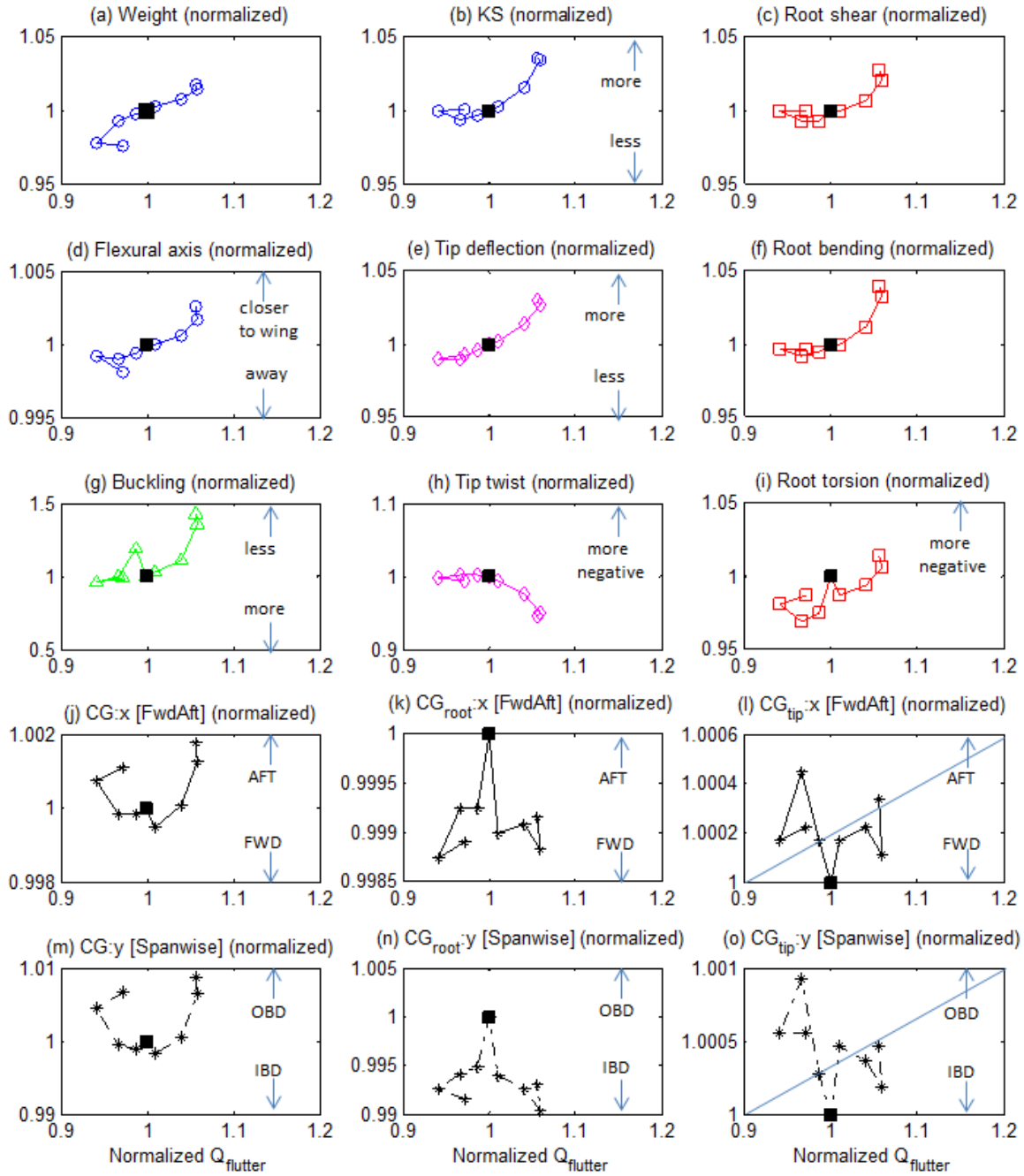


Figure 29. Data for group E (rib orientation). Plots crossed out have less than 0.1% range on the x- and y-axes.

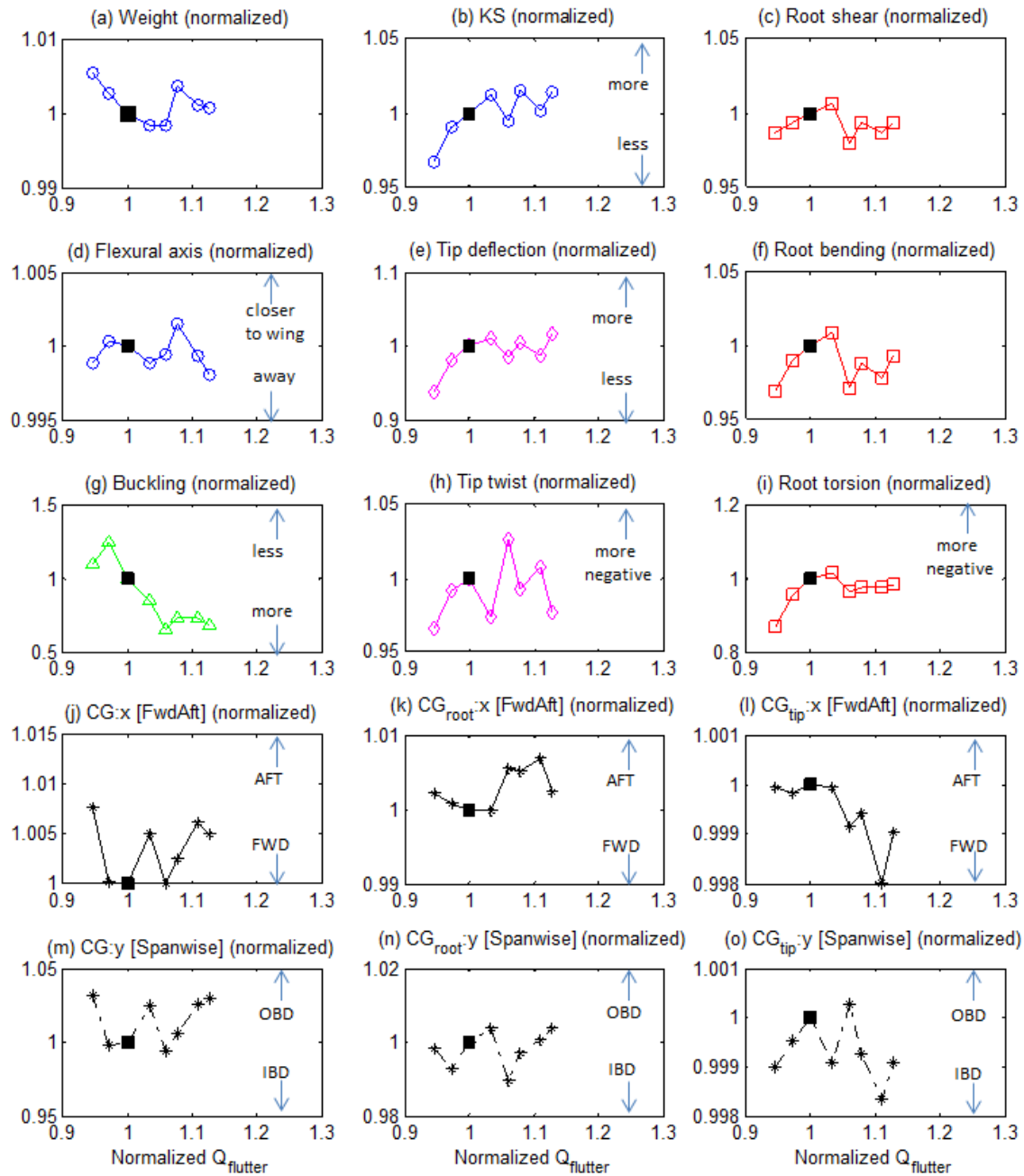


Figure 30. Data for group F (large flutter range).

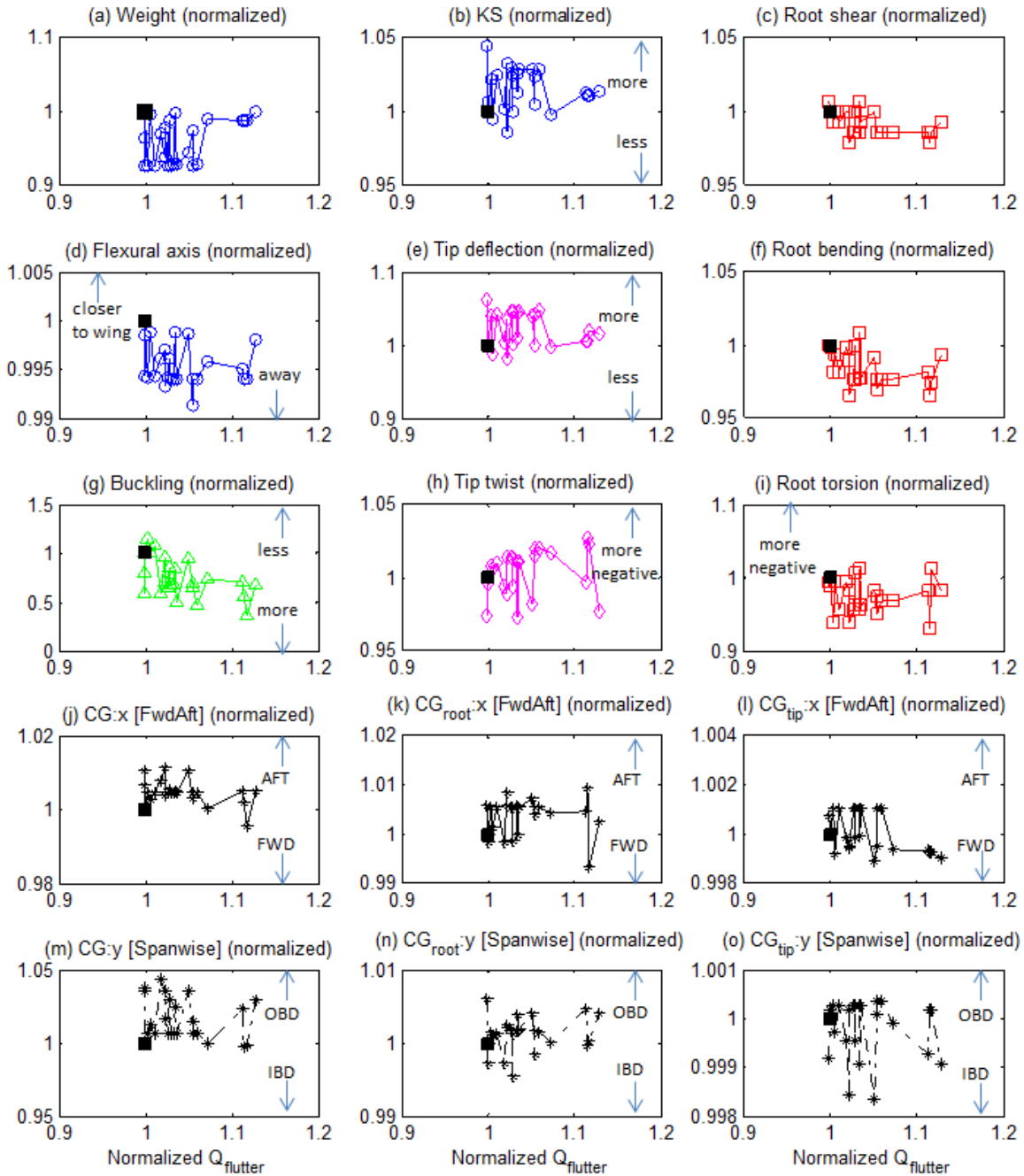


Figure 31. Data for group G (improved weight and flutter speed).

Given what was observed with the conflicting wash-in and wash-out trends seen above, it would seem that a high performing curvilinear spar design (which displays more wash-out than the baseline) would conflict with the highest performing rotated rib design (which displays more wash-in than the baseline) to create a wing design of lower flutter resistance than at least one of these two original designs. To explore this, a wing was created which used rotated ribs at 24 degrees (the best seen in the rib orientation studies) and a high performing inner spar configuration, i.e. $[p2_o, p3_o] = [0.9, 0.1]$ and $[p4_i, p5_i, p6_i, p5_o, p6_o] = [0.25, 1, 4, 4, 4]$.

The results are summarized in Table 18, and the values represent percent differences when compared to the baseline. Looking at the data most influenced by the stiffness (flexural axis, tip deflection, and tip twist), the two designs have clearly differing values as anticipated. Looking at the data most influenced by the mass, the two designs differ once again, since the rib design has its root mass forward of the baseline and its tip mass aft of the

baseline. The spar design is just the opposite. The movement of the tip mass will have a greater impact on flutter speed than the root mass. Although these designs seem to have different means for increasing their flutter resistance over the baseline, when combined, their respective increases in flutter speeds essentially add to create a design with even higher resistance to flutter.

In the resulting design (provided in the last row of the table), the tip mass moves forward, which has been seen to increase the flutter speed with the spar studies. The flexural axis moves away from the wing, indicating more wash-out than the baseline; however, the tip twist value is negative, corresponding to less negative twisting compared to the baseline, which indicates more wash-in behavior than the baseline (at least at the tip). Additionally, when observing the KS values of the two designs, one is positive and one is negative. Typically, for the other metrics in the table (besides flutter), the result for the combined design is somewhere between the two values of the original designs, but here, the resulting KS value for the combined design has a higher absolute value than either of the other designs it comprises.

Table 18. Percent differences with respect to the baseline of three designs, where the first two designs combine to make the third design.

Design	Weight	KS	Flutter speed	Stiffness			Mass	
				Flexural axis*	Tip def.	Tip twist **	CG _{root} (+ = aft)	CG _{tip} (+ = aft)
Ribs rotated	1.5	3.8	5.8	0.2	2.7	-4.8	-0.12	0.01
Curved spar	-1.0	-0.5	9.3	-0.5	-0.2	2.4	0.44	-0.07
Combination	0.5	4.4	15.5	-0.2	2.6	-1.9	0.33	-0.05

* Flexural axis: Positive value indicates flexural axis moving toward wing (more wash-in expected)
 ** Tip twist: Positive value indicates increased negative twist (more wash-out expected)

One final comparison was made to uncover a potential correlation; the separation in natural frequencies of wing designs. The natural frequencies are affected by both the wing mass distribution and stiffness distribution. The onset of flutter typically occurs as two wings modes begin to coalesce. Therefore the first and second bending modes (1B and 2B) and the first torsional mode (1T) for groups A and F were calculated. Figure 32 shows the results when comparing the differences between (1B and 1T) and (2B and 1T). Both have a slight negative trend (meaning the separation in the modal frequencies decrease) as the flutter speed increases. This again is counterintuitive because the expected trend is positive, where a larger separation in the modes would be expected to delay the onset of flutter [13]. Once again, this example and the example described in Table 18 demonstrate the difficulties of discovering design trends for improving flutter resistance.

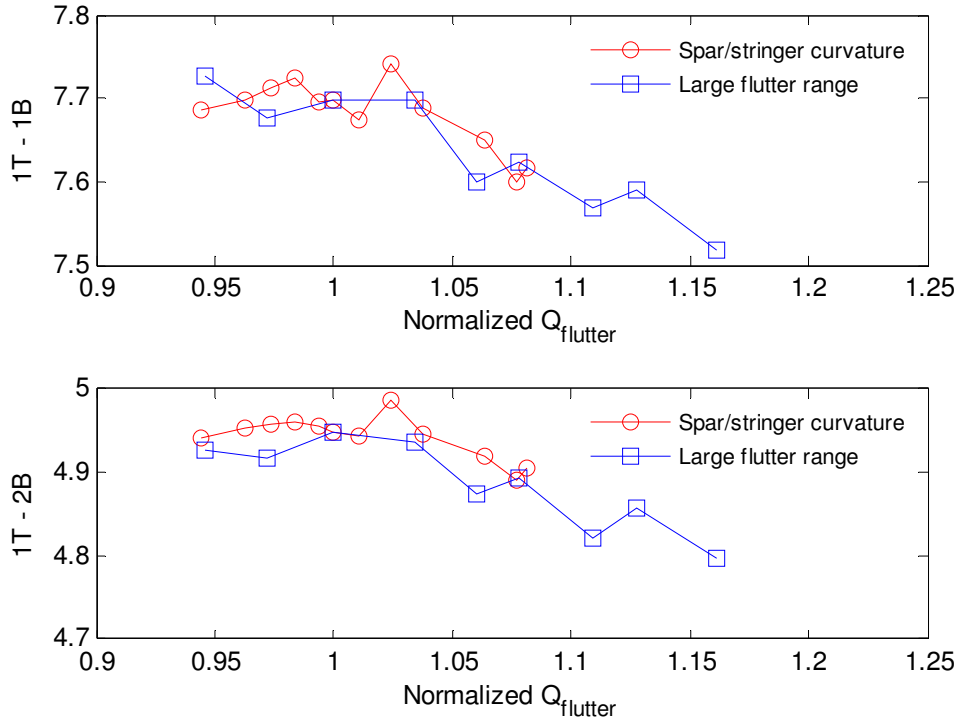


Figure 32. Comparing the separation of natural modes to normalized $Q_{flutter}$ for two groups of designs, spar/stringer curvature (group A) and larger flutter range (group F).

VIII. Parameter Studies Summary

This section compares the best designs of the individual studies above (#1-12) and illustrates which spar and rib configurations are most effective. To help illustrate the relative performance between designs highlighted earlier, Figure 33 plots the best designs of those parametric studies which showed significant improvement (higher flutter speed and/or lower weight) over the baseline. The legend in the figure identifies the studies from which the data points originated. The last entry in the legend is a group of designs that were created from combining designs generated from the separate studies on rib, spar, and stringer modifications. For consistency, when creating these new designs, only those designs which had a maximum p4-p6 value of 4 were considered (eliminating the use of designs from study #2 which had a maximum p4-p6 value of 10). Table 19 provides the design parameter values and the performance results for many of the designs shown in Figure 33. Finally, Figure 34 illustrates six designs, most of which are new designs, to help aid the discussion on superior rib and spar configurations.

For the spar/stringer designs (studies #2 - #5 in Figure 33), the best curvature definition parameters (i.e., p4, p5_i, p6_i, p5_o, p6_o) of study #3 is design 'c', whose flutter speed vs. weight data point was located in the upper left corner of an earlier figure, Figure 10(b). Table 19 shows that the curvature definition parameters for the outboard section of the spar (i.e., p6_i, p5_o, p6_o) are all equal and greater than one (i.e., [4, 4, 4]), defining the spar as straight and shifted toward the leading edge in the outboard section of the wing. It can be seen from study #3's data that this topology for the outboard section of the wing (i.e., p6_i = p5_o = p6_o = 4) was consistent across the four highest data points found in Figure 10(b). For study #3, the design having no spar curvature (i.e., all five curvature definition parameters equal to 4) failed to mesh successfully. However, for comparison purposes, the two best designs of study #2 (design 'a' and 'b' in Figure 33) also had a straight spar in the outboard wing section, and further, design 'b' had a straight spar in the inboard section (i.e., the five curvature definition parameters all equaled 10). As discussed earlier, the curvilinearity of the spar/stringers does not seem to provide additional benefit over a straight configuration with respect to flutter resistance. Additionally, these designs ('a' and 'b') have a higher flutter speed than design 'c', as shown Figure 33, suggesting that for higher flutter resistance it is more important to shift the weight forward and less important to have curvilinear spar/stiffeners.

Figure 33 and Table 19 also show that by enabling the curvature definition parameters ($p_4 - p_6$) to have the values of 0.25, 1, and 4, the spar/stringers can shift forward (and aft) by a certain amount. After reaching the maximum forward position, the control line parameters enabled the spar/stringer designs to bend even further forward. In study #5, although the inner spar was not included, the trend showed that the best designs, which had straight stringers in the outboard, could be improved by updating the control line parameters from [0.5, 0.5] to [0.9, 0.1] in the outboard. Figure 13, shown previously, illustrates how these control line parameters bend the straight spar/stringer of the outboard wing section forward. This set of control line parameters was applied to design 'c' to create an improved design (design 'f'). Design 'f' and its counterpart design that has no inner spar, design 'd', are used in every case in designs 'm' - 'r' shown in Figure 34.

Considering the rib studies that held the number of ribs constant (studies #7 and #9 - 12), study #7 had an increased flutter resistance (and increased weight) when the straight ribs were oriented at 24 degrees (design 'g'). Study #9 had two designs ('h' and 'i' in Figure 33) with relatively high flutter speeds where both designs had convex ribs whose control line locations caused the ribs to have the majority of their length angled near 26 degrees. Concave designs were also shown to have better flutter resistance when their control line locations caused more rib length to be oriented along 26 degrees, but these designs were not better than design 'h' and 'i'. Design 'h' (illustrated earlier in Figure 16), has slightly less weight than the baseline, where design 'i' has more weight than the baseline. Designs 'j' and 'k' of study #10 are less weight than the baseline mostly due to the removal of the inner spar and utilize the rib configuration of design 'i'. Design 'j' was illustrated previously in Figure 19. In study #12, when the spar and rib designs were combined, the best spar/stringer configuration (design 'f') was combined with the rib configuration of design 'h', to create a more superior design, design 'm', which was illustrated in Figure 24. This design is also shown in Figure 34. The rib configurations of either designs 'g', 'h', and 'i' are used in all but one case (design 'n') in the high performing designs of Figure 34.

Design 'n' was another superior design of study #12. However, design 'n' is trivial in that the ribs are both straight and shifted outboard ($p_4=p_5=p_6=4$) making them shorter in both length and depth, such that they are the lightest rib configuration possible when modifying the curvature definition parameters ($p_4 - p_6$). This design happens to have a higher flutter speed than the baseline due to its spar configuration 'f'. When exploring how a design having baseline spars and curvilinear ribs (like design 'h', whose rib configuration is found in design 'm' in Figure 34) can have a lower weight than the baseline, design 'n' with the straight ribs provides some insight. In particular, the curvature definition parameters of design 'h' are all greater than or equal to unity, i.e. [4, 1, 4], such that the endpoints of all the ribs are shifted outboard, just as they were with design 'n' when the ribs became geometrically smaller, resulting in less weight.

Designs 'o' and 'p' (shown in Figure 34) were created from the rib configurations of designs 'g' and 'i', respectively, by updating the baseline spar/stringer configuration to the lighter weight and higher flutter speed design of design 'f'. Designs 'o' and 'p', although slightly heavier than the baseline (by $\leq 0.6\%$), are worth showing here since their flutter speeds reach 16.1% improvement over the baseline. Designs 'q' and 'v' are essentially designs 'p' and 'o' with no inner spar, respectively. Design 'q' is shown in Figure 34.

For a similar reason, designs 'r', 't', and 'u' were created to further investigate curvilinear ribs, since curvilinear ribs will always have more weight than their straight rib counterparts for the same number of ribs, unless the ribs are rotated normal to the leading edge or shifted outboard within a tapered wing like the CRM. Since curvilinear ribs are essentially longer, fewer of them may be needed to support the overall wing structure. Therefore, five ribs were eliminated from the outboard section of design 'p' to create design 'r' (shown in Figure 34). Here the new design is about the same weight as the baseline and still has a 12.6% increase in the flutter speed. By removing some ribs, the stresses increased by 0.2% over that of design 'p' and resulted in a 0.6% increase in KS over the baseline.

Additionally, to compare design 'i' (a curvilinear design) and design 'g' (a rotated straight-rib design) to the baseline, ten ribs were removed from the outboard of design 'i' to create design 't', and nine ribs were removed from the outboard of design 'g' to create design 'u'. The resulting designs are very close to the baseline weight, and although the flutter speed reduced, the curvilinear design, design 't', still has a 2.1% increase in the flutter speed where the straight-rotated rib design has only a 0.4% increase in flutter speed. Interestingly, design 't' has a lower flutter speed than design 'h' (a curvilinear design mentioned previously). This implies that the additional weight from design 'i', not only its curvature, helps it have the highest flutter value of study #9. Yet curvature is still playing an important role here since there are many designs in study #9 that have higher weight than design 'i' but a lower flutter speed.

When using the same set of parameter values to modify the spar/rib curvatures, the spars (and stringers) proved to be more effective in increasing the flutter speed of the designs than the ribs. For example, design 'f' (which has spar/stringer modification only) had a 9.3% improvement in the flutter speed and a 0.5% decrease in KS, where design 'h' (which has rib modification only) had a 3.4% improvement in flutter speed and a 1.2% increase in KS.

Design 'e' (which had stringer modifications only and no inner spar) had a 6.0% improvement in the flutter speed and a 2.8% increase in KS which is expected given the larger weight decrease of 7.1%. Design 'f' and design 'h' only had a 1.0% and 0.2% decrease in weight, respectively. The spars and stringers may be more effective in increasing the flutter speed than the ribs since they are aligned more with the load path, even when ribs are curved or reoriented. This enables the spars and stringers to have both an inertial and stiffness impact, compared to the ribs which primarily only have an inertial impact.

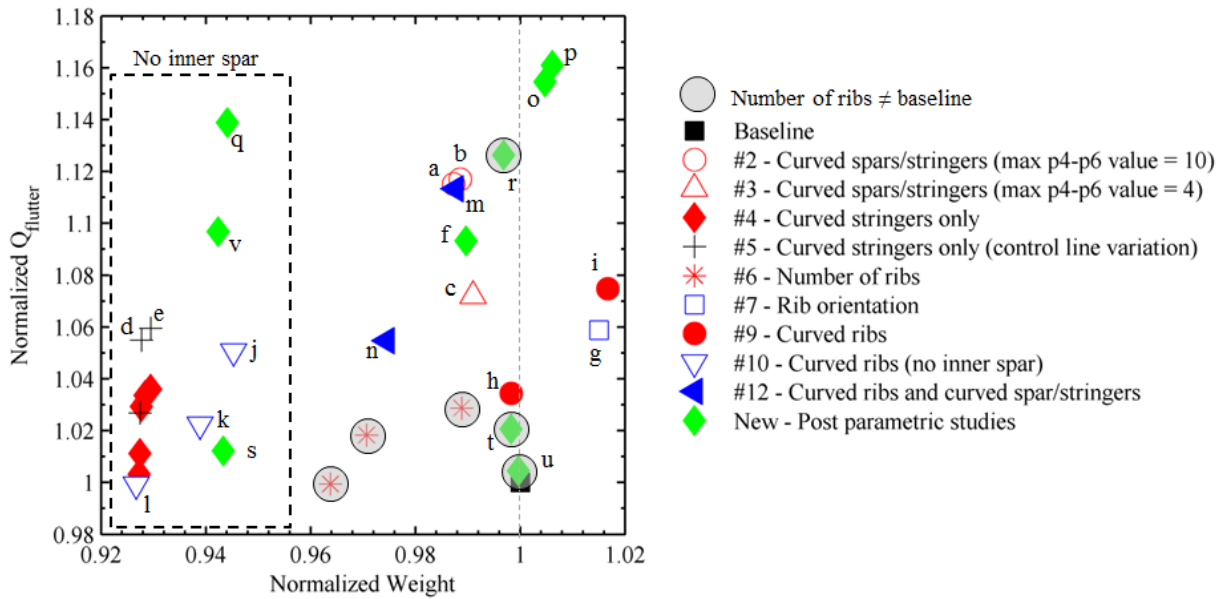


Figure 33. The best designs of the parametric studies along with nine new designs. The numbers in the legend indicate which of the twelve parametric studies the design came from. The dashed box indicates the designs having no inner spar.

Table 19. Summary of the best designs of the parametric studies along with nine new designs.

Study	Design	Spar/stringers		Ribs (IBD = OBD)	Weight (%)	Flutter	
		(p2 _o ,p3 _o)	[p4 _i ,p5 _i ,p6 _i ,p5 _o ,p6 _o]	(p2 _o ,p3 _o)		Speed (%)	KS (%)
#2	a	(0.5, 0.5)	[0.1, 0.1, 10, 10, 10]	- baseline -	-1.3	11.5	1.1
	b	(0.5, 0.5)	[10, 10, 10, 10, 10]	- baseline -	-1.1	11.7	1.1
#3	c	(0.5, 0.5)	[0.25, 1, 4, 4, 4]	- baseline -	-0.9	7.2	-0.2
#5	d	(0.9, 0.1)	[0.25, 1, 4, 4, 4]	- baseline -	-7.2	5.5	2.4
	e	(0.9, 0.1)	[4, 0.25, 4, 4, 4] (no spar)	- baseline -	-7.1	6.0	2.8
new	f	(0.9, 0.1)	[0.25, 1, 4, 4, 4]	- baseline -	-1.0	9.3	-0.5
#7	g	- baseline -		Straight at 24 degrees	1.5	5.8	3.8
#9	h	- baseline -		(0.2, 0.2) [4, 1, 4]	-0.2	3.4	1.2
	i	- baseline -		(0.2, 0.2) [4, 0.25, 1]	1.7	7.5	-0.1
#10	j	(baseline with no spar)		Same as i	-5.5	5.1	2.9
	k	(baseline with no spar)		(0.5, 0.5) [4, 0.25, 1]	-6.1	2.2	3.3
	l	(baseline with no spar)		Same as h	-7.3	-0.1	4.4
#12	m	Same as f		Same as h	-1.2	11.3	1.3
	n	Same as f		(0.5, 0.5) [4, 4, 4]	-2.6	5.5	0.4
new	o	Same as f		Same as g	0.5	15.5	4.4
new	p	Same as f		Same as i	0.6	16.1	0.4
new	q	Same as d		Same as i	-5.6	13.9	3.0
new	r	Same as f		Same as i (5 less OBD ribs)	-0.3	12.6	0.6
new	s	(baseline with no spar)		Same as g	-5.7	1.2	7.1
new	t	- baseline -		Same as i (10 less OBD ribs)	-0.2	2.1	0.3
new	u	- baseline -		Same as g (9 less OBD ribs)	0.0	0.4	1.6
new	v	Same as d		Same as g	-5.8	9.7	7.3

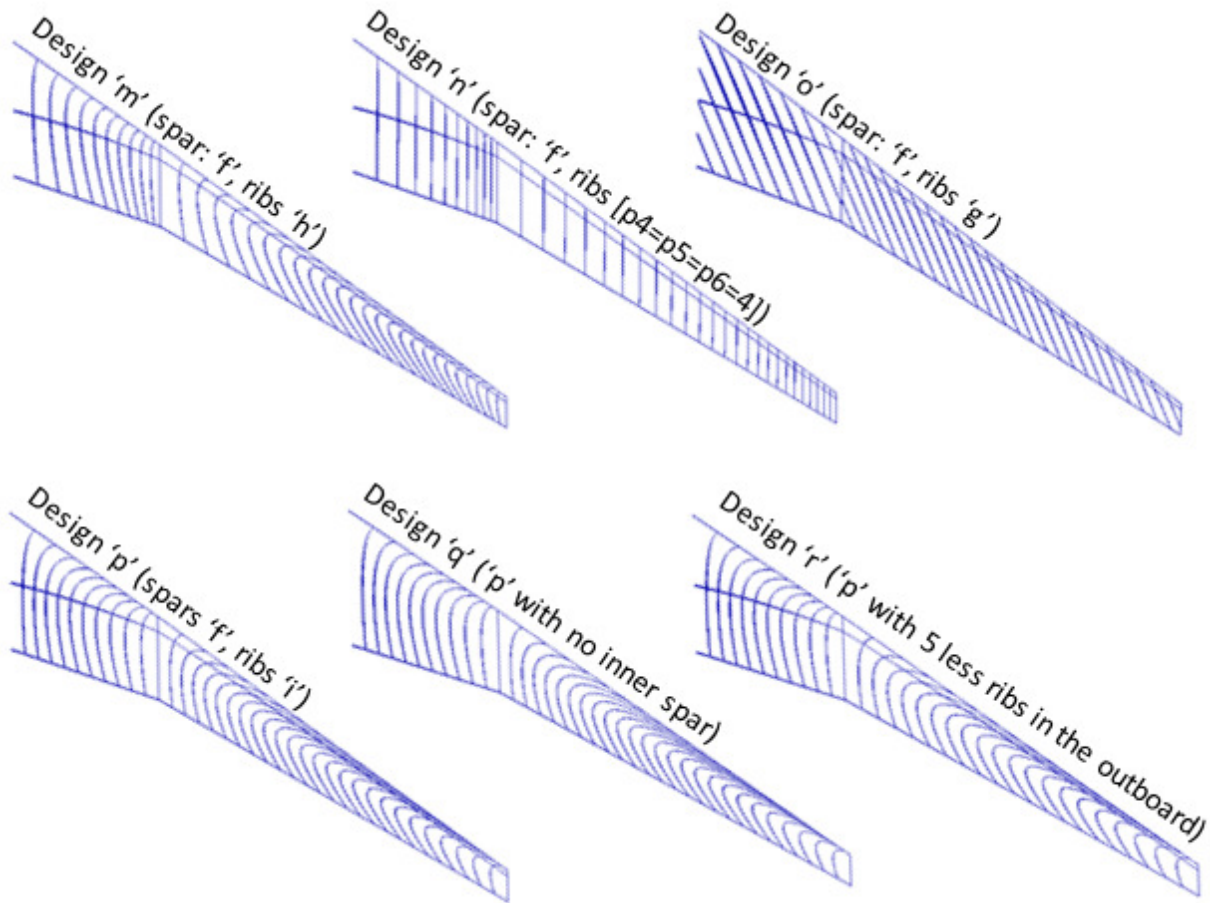


Figure 34. Six designs having relatively high performance in either weight reduction or flutter resistance.

IX. Conclusions and Outlook

In this work, a fully-populated wing box structure within the CRM wing is used as a baseline. An aeroelastic framework of MATLAB, PATRAN, and NASTRAN modules is used to compute the static aeroelastic response and the dynamic aeroelastic flutter boundary of a given wing structure. Twelve parametric studies were performed on the baseline wing's spars, ribs, and stringers to help identify which changes to the internal structure design have the greatest effect on both increasing the wing's flutter resistance and in decreasing its weight. The parameters used in these studies allowed for both straight and curvilinear structural members. Additional evaluation metrics were considered to detect design trends that lead to lighter-weight, aeroelastically stable wing designs, where the results here are specific to the CRM and similar wing designs.

Since the focus of this research is weight reduction, it would have been useful to hold the flutter speed constant during a parametric study and monitor the subsequent allowable weight change, but this is very challenging (without optimization). Instead it was typically effective to hold the number of structural components constant (which consequently minimized the weight range among the designs) and compare the relative changes in flutter results. With this approach, although the resulting designs have similar weight, it can be inferred that designs having higher flutter speeds should be capable of a lower weight, than designs with lower flutter speeds. However, multiple metrics, such as the effect on static aeroelastic stresses and skin bucking, also need to be taken into account, which tends to complicate these inferences.

By varying the spar, stringer, and rib configurations, some designs were created that simultaneously had less weight and higher flutter resistance than the baseline model. The best of these designs are included in Figure 33 and Table 19. Two designs, which modified the curvature of the spars and stringers, (design 'c' and design 'f') showed improvement in the KS value, weight, and flutter values. The combination of a lower weight, higher flutter

resistance, and lower stresses was rarely observed. Of the designs in Table 19, the largest increase in the KS value using curvilinear members was 4.4%. For straight-rotated members, the largest increase was 7.3%, but some of this stress may have been due to the configuration of the baseline, where the rib between the inboard and outboard sections remains straight, causing the rotated straight ribs to attach to it. If this rib was eliminated, the rotated ribs would remain continuous, potentially decreasing the stresses. Design 'o' in Figure 34 shows the connectivity between the straight-rotated ribs at the boundary between the inboard and outboard ribs.

When using the same set of parameter values to modify the spar/rib curvatures, the spars (and stringers) proved to be more effective in increasing the flutter speed of the designs. For example, design 'f' (which has spar/stringer modification only) had a 9.3% improvement in the flutter speed and design 'e' (which had stringer modifications only and no inner spar) had a 6.0% improvement in flutter speed. Design 'h' (which has rib modification only) had a 3.4% improvement in flutter speed. Of these three designs, the stringer-only design had the greatest stress but also the greatest weight reduction due to the removal of the inner spar. The spars and stringers may be more effective in increasing the flutter speed than the ribs since they are aligned more with the load path, even when ribs are curved or reoriented. This enables the spars and stringers to have both an inertial and stiffness impact, compared to the ribs which primarily only have an inertial impact.

When modifying the spar and stringers (not the ribs), the straight designs performed just as well as the curvilinear designs, since the weight and flutter improvements resulted mostly from shifting the spanwise structural members forward (e.g., designs 'a' and 'b'). Here, it was most beneficial to straighten the spar and stringers so that a majority of their length was closer to the leading edge. At times curvature did help improve the wing's flutter resistance, but this was only when the curvature allowed the spar to bow closer to the leading edge (e.g., design 'c' which has a straight spar in the outboard wing section was modified to have slight curvature, resulting in design 'f' which has a higher flutter speed than design 'c'). A straight spar would still outperform this design if its location was closer to the leading edge (e.g., design 'b' has a straight spar closer to the leading edge than design 'f', which has a slightly curved spar.) When considering buckling, it was found that the straight spar design had a 10% reduction in buckling resistance. To maintain the buckling resistance of the baseline yet improve the flutter speed, a particular design used a straight, equally-spaced spar and stringer configuration in the inboard section (to improve the support of the skins near the wing root) and a curved, forward-shifted spar and stringers configuration in the outboard (to increase the wing's stability).

When modifying the ribs only (not the spar and stringers), the best designs had a majority or all of the rib lengths oriented at roughly 24-26 degrees (e.g., designs 'g', 'h', and 'i'). Designs 'g' and 'i' showed that the straight rib designs performed similarly to the curved rib designs, respectively. The straight rib design had more stress but as mentioned above this may have been due to the configuration of the baseline. The curved rib designs had relatively higher weight than the baseline, unless the curved ribs were shifted outboard (design 'h') due to the values of the curvature definition parameters (p_4 - p_6) or the number of ribs was reduced (design 'r', 't', and 'u'), which may be feasible since fewer ribs may be sufficient when their relative length is greater. Three designs ('h', 't', and 'u') had similar weight as the baseline. These designs showed at most a 3.4% increase in the flutter speed. The third design ('u') had straight-rotated ribs and showed only a 0.4% improvement in the flutter speed. The second design ('t') had a lower flutter speed (and ten fewer ribs) than the first design, which meant that before the ten ribs were removed, the design's flutter speed (i.e., the flutter speed of design 'i') was affected by both rib curvature and the additional weight and stiffness from the extra ribs.

For the topology work, large weight reductions were obtained by removing an inner spar, and performance was maintained by shifting stringers forward and/or using curvilinear ribs: 5.6% weight reduction, a 13.9% improvement in flutter speed, but a 3.0% increase in stress levels (design 'q'). Performance was also maintained (for flutter speed, not stress) using rotated-straight ribs (design 'v') but the design had a 4.2% lower flutter speed than the curved ribs of similar weight (design 'q').

By exploring obvious trends in the data, no evaluation metric consistently correlated with weight or flutter speed; however, some trends were detected when comparing designs that had gradual changes in structural configuration from one design to the next, as opposed to picking random designs of varying topology to compare. An expected trend found from the data was that a decrease in weight typically resulted in more tip deflection and higher stresses. It appeared that some wing designs used wash-in to increase flutter resistance (rotated rib designs), which is the expected trend, while other designs used wash-out (spar/stringers designs). However, when these differing groups of design were merged together, their benefits surprisingly complimented one another (neglecting stress). As permutations to the wing designs were made, both the inertial and stiffness distributions changed, making it difficult to find design trends that showed consistent correlation with an increase in flutter resistance.

The results of these parametric studies provided additional insight into the following:

- The addition of spars increases the flutter resistance of the wing with a corresponding weight penalty. When spars are located toward the leading edge, the flutter speed increases, such that a wing design with 4 spars (and 4 stringers) can have the same flutter resistance as a wing design with 8 spars (and 0 stringers). This follows a well-known trend of pushing the CG forward for better flutter resistance [13].
- The outboard wing section, especially the wing tip, was the most sensitive region for aeroelastic tailoring. For this design space, inertial forces (which are most readily impacted by adding/altering material at the wing tip) are playing a greater role than elastic forces (which are more sensitive to changes at the wing root, where the bending and torsional stresses will be largest).
- When modifying the number of straight ribs in a design, there were a few designs with lower weight and higher flutter speed than the baseline, but they required fewer ribs in the inboard and more ribs in the outboard, making the rib spacing quite different between the two wing sections. It is likely this rib configuration increased the wing's resistance to flutter by lowering the frequency of the first bending mode [13]. However, this rib arrangement potentially creates other problems such as buckling or outer mold line distortion.
- When rotating straight ribs, there were clear trends between weight and flutter, with a maximum flutter speed at 24 degrees and minimum at -36 degrees; however, no design was superior to the baseline in both weight and flutter speed. Similar results were found in [7]. The design having ribs oriented at -36 degrees is a standard rib configuration, i.e. ribs are perpendicular to the wing leading edge, which is recommended for weight reduction [14]. This design had 2% less weight than the baseline, where the design having maximum flutter speed had 1.5% more weight than the baseline.
- When investigating the effect of rib curvature, the most insight came by comparing designs that had the same curvature definitions (which defined the general curvature as concave or convex) but different control lines (where the control line defined the location of maximum curvature in a rib or spar). Four example cases were considered. Regardless of the direction of the curve (concave or convex), the best designs had a large portion of their curved ribs aligned near 26 degrees. The locations of control lines caused the rib curvatures to align the majority of their rib length at approximately the same orientation as the best design from the rotated, straight-ribs study.
- When evaluating the effect of curved ribs with stringer-only designs, the flutter speed decreased by 2-8% due to removal of the inner spar. Initial studies suggest that for the same weight, designs having more rib curvature tend to have less of a flutter penalty in the absence of the inner spar.
- When combining a high-performing spar design with a high-performing rib design (where the performance is measured with respect to weight and flutter), the resulting designs complimented one another to produce a higher performing design in terms of flutter resistance and weight reduction than the two designs it comprises (neglecting changes in stress).

Since the design evaluations in this work are based on comparisons with a baseline model, the resulting trends are less sensitive to modeling inaccuracies, such as finite element model discretization errors, undetected transonic effects, and any other modeling omission. In other words, each potential inaccuracy may shift individual flutter points but would likely not impact the comparative metrics being used here.

Allowing the ribs, stringers, and spars to curve resulted in greater tailorability of the structural performance and provided some designs where all three parameters, weight, flutter point, and KS values, were all improved. The tradeoffs between straight and curvilinear members are significant enough that formal design optimization is the best next step. A design optimization routine could exploit the trade-offs and remove weight where possible to drive toward lower weight designs that still satisfy the design constraints, including flutter stability, static aeroelastic stresses, and skin buckling. While buckling was considered occasionally in this work, future studies will incorporate a larger emphasis on skin buckling. Already, an optimization framework is being developed by collaborators at Virginia Tech who are considering these various trade-offs and employing curvilinear spars, ribs, and stiffeners where advantageous.

Acknowledgements

This work is funded by the Fixed Wing project under NASA's Fundamental Aeronautics Program.

References

- [1] Taminger, K., Hafley, R., "Electron Beam Freeform Fabrication: A Rapid Metal Deposition Process." *Proceedings of the 3rd Annual Automotive Composites Conference*, Troy, MI, September 9-10, 2003.
- [2] Dang, T., Kapania, R., Slemple, W., Bhatia, M., Gurav, S., "Optimization and Postbuckling Analysis of Curvilinear-Stiffened Panels Under Multiple-Load Cases," *Journal of Aircraft*, Vol. 47, No. 5, pp. 1-12, 2010.
- [3] Bhatia, M., Kapania, R., Evans, D., "Comparative Study on Optimal Stiffener Placement for Curvilinearly Stiffened Panels," *Journal of Aircraft*, Vol. 48, No. 1, pp. 77-91, 2011.
- [4] Locatelli, D., Mulani, S., Kapania, R., "Wing-Box Weight Optimization Using Curvilinear Spars and Ribs (SpaRibs)," *Journal of Aircraft*, Vol. 48, No. 5, pp. 68-79, 2011.
- [5] Balabanov, V., Haftka, R., "Topology Optimization of a Transport Wing Internal Structure," AIAA Paper 94-4414.
- [6] Kobayashi, M., Pedro, H., Kolonay, R., Reich, G., "On a Cellular Division Method for Aircraft Structural Design," *The Aeronautical Journal*, Vol. 113, No. 1150, pp. 821-831, 2009.
- [7] Harmin, M., Ahmed, A., Cooper, J., Bron, F., "Aeroelastic Tailoring of Metallic Wing Structures," *AIAA Structures, Structural Dynamics and Materials Conference*, Denver, Colorado, April 4-7, 2011.
- [8] Vassberg, J., DeHaan, M., Rivers, S., Wahls, R., "Development of a Common Research Model for Applied CFD Studies." *AIAA Applied Aerodynamics Conference*, Honolulu, HI, August, 2008.
- [9] Kreisselmeier, G., Steinhauser, R., "Systematic Control Design by Optimizing a Vector Performance Index", *International Federation of Active Controls Symposium on Computer-Aided Design of Control Systems*, Zurich, Switzerland, 1979.
- [10] Weisshaar, T., Nam, C., Batista-Rodriguez, A., "Aeroelastic Tailoring for Improved UAV Performance," *AIAA Structures, Structural Dynamics, and Materials Conference*, Long Beach, CA, April 20-23, 1998.
- [11] Box, G.E., Hunter, J.S., Hunter, W.G. *Statistics for Experimenters: Design, Innovation, and Discovery, 2nd Edition*, Wiley, Hoboken, New Jersey, 2005.
- [12] Locatelli, D., "Optimization of Supersonic Aircraft Wing-Box Using Curvilinear SpaRibs," PhD Dissertation, Virginia Polytechnic Institute and State University, 2012.
- [13] Bisplinghoff, R., Ashley, H., Halfman, R., *Aeroelasticity*, Dover Publications, Mineola, NY, 1996.
- [14] Niu, M., *Airframe Structural Design*, Hong Kong Conmilit Press, Hong Kong, 1988.

REPORT DOCUMENTATION PAGE			Form Approved OMB No. 0704-0188		
<p>The public reporting burden for this collection of information is estimated to average 1 hour per response, including the time for reviewing instructions, searching existing data sources, gathering and maintaining the data needed, and completing and reviewing the collection of information. Send comments regarding this burden estimate or any other aspect of this collection of information, including suggestions for reducing this burden, to Department of Defense, Washington Headquarters Services, Directorate for Information Operations and Reports (0704-0188), 1215 Jefferson Davis Highway, Suite 1204, Arlington, VA 22202-4302. Respondents should be aware that notwithstanding any other provision of law, no person shall be subject to any penalty for failing to comply with a collection of information if it does not display a currently valid OMB control number.</p> <p>PLEASE DO NOT RETURN YOUR FORM TO THE ABOVE ADDRESS.</p>					
1. REPORT DATE (DD-MM-YYYY) 01-03 - 2015		2. REPORT TYPE Technical Memorandum		3. DATES COVERED (From - To)	
4. TITLE AND SUBTITLE Internal Structural Design of the Common Research Model Wing Box for Aeroelastic Tailoring			5a. CONTRACT NUMBER		
			5b. GRANT NUMBER		
			5c. PROGRAM ELEMENT NUMBER		
6. AUTHOR(S) Jutte, Christine V.; Stanford, Bret K.; Wieseman, Carol D.			5d. PROJECT NUMBER		
			5e. TASK NUMBER		
			5f. WORK UNIT NUMBER 081876.02.07.02.01.03		
7. PERFORMING ORGANIZATION NAME(S) AND ADDRESS(ES) NASA Langley Research Center Hampton, VA 23681-2199			8. PERFORMING ORGANIZATION REPORT NUMBER L-20534		
9. SPONSORING/MONITORING AGENCY NAME(S) AND ADDRESS(ES) National Aeronautics and Space Administration Washington, DC 20546-0001			10. SPONSOR/MONITOR'S ACRONYM(S) NASA		
			11. SPONSOR/MONITOR'S REPORT NUMBER(S) NASA-TM-2015-218697		
12. DISTRIBUTION/AVAILABILITY STATEMENT Unclassified - Unlimited Subject Category 01 Availability: NASA STI Program (757) 864-9658					
13. SUPPLEMENTARY NOTES					
14. ABSTRACT This work explores the use of alternative internal structural designs within a full-scale wing box structure for aeroelastic tailoring, with a focus on curvilinear spars, ribs, and stringers. The baseline wing model is a fully-populated, cantilevered wing box structure of the Common Research Model (CRM). Metrics of interest include the wing weight, the onset of dynamic flutter, and the static aeroelastic stresses. Twelve parametric studies alter the number of internal structural members along with their location, orientation, and curvature. Additional evaluation metrics are considered to identify design trends that lead to lighterweight, aeroelastically stable wing designs. The best designs of the individual studies are compared and discussed, with a focus on weight reduction and flutter resistance. The largest weight reductions were obtained by removing the inner spar, and performance was maintained by shifting stringers forward and/or using curvilinear ribs: 5.6% weight reduction, a 13.9% improvement in flutter speed, but a 3.0% increase in stress levels. Flutter resistance was also maintained using straight-rotated ribs although the design had a 4.2% lower flutter speed than the curved ribs of similar weight and stress levels were higher. For some configurations, the differences between curved and straight ribs were smaller, which provides motivation for future optimization-based studies to fully exploit the trade-offs.					
15. SUBJECT TERMS Aeroelastic tailoring; Curvilinear structures; Topology; Transport aircraft					
16. SECURITY CLASSIFICATION OF:			17. LIMITATION OF ABSTRACT	18. NUMBER OF PAGES	19a. NAME OF RESPONSIBLE PERSON
a. REPORT	b. ABSTRACT	c. THIS PAGE			STI Help Desk (email: help@sti.nasa.gov)
U	U	U	UU	48	19b. TELEPHONE NUMBER (Include area code) (757) 864-9658